J. Fluid Mech. (2011), *vol.* 685, *pp.* 461–494.
doi:10.1017/jfm.2011.331

Cylinder rolling on a wall at low Reynolds numbers

Alain Merlen and Christophe Frankiewicz†

Joint International Laboratory LEMAC, Institut d'Électronique Microélectronique et Nanotechnologie UMR CNRS 8520, Université des Sciences et Technologies de Lille, Ecole Centrale de Lille, France

(Received 24 November 2010; revised 18 April 2011; accepted 1 August 2011; first published online 22 September 2011)

The flow around a cylinder rolling or sliding on a wall was investigated analytically and numerically for small Reynolds numbers, where the flow is known to be two-dimensional and steady. Both prograde and retrograde rotation were analytically solved, in the Stokes regime, giving the values of forces and torque and a complete description of the flow. However, solving Navier–Stokes equation, a rotation of the cylinder near the wall necessarily induces a cavitation bubble in the nip if the fluid is a liquid, or compressible effects, if it is a gas. Therefore, an infinite lift force is generated, disconnecting the cylinder from the wall. The flow inside this interstice was then solved under the lubrication assumptions and fully described for a completely flooded interstice. Numerical results extend the analysis to higher Reynolds number. Finally, the effect of the upstream pressure on the onset of cavitation is studied, giving the initial location of the phenomenon and the relation between the upstream pressure and the flow rate in the interstice. It is shown that the flow in the interstice must become three-dimensional when cavitation takes place.

Key words: low-Reynolds-number flows, microfluidics, vortex flows

1. Introduction

A cylinder placed transversally in a free stream is one of the most studied flows. This has been motivated by its wide relevance to many application fields and also by its simple geometry for easier numerical and theoretical approaches. Most of the application examples, from civil engineering to aerodynamics and fluid–structure interaction, have concerned high-Reynolds-number flows and unsteady interactions between the wake and the surroundings. Recently, with the development of microtechnology, microfluidics has brought renewed attention to low-Reynolds-number flows around rotating cylinders and particularly in microchannels where the interaction with walls is strong. For low Reynolds number flows, numerical results can sometimes be compared with analytical solutions obtained under Stokes flow assumptions, improving the results when solving delicate issues like the contact problem between a rolling cylinder and a wall. The present paper answers that problem and gives a detailed description of the flow squeezed between a rotating cylinder and a wall for a wide range of situations including the onset of cavitation. It also provides reference Stokes solutions for the global flow around a cylinder rolling

† Email address for correspondence: christophefrankiewicz@msn.com

on a translating wall with an arbitrary slip. A global model of the contact area was derived so that it could be implemented in numerical two-dimensional computations as one contact point instead of a time-consuming discretization of the interstice. Finally, the paper presents an analysis of the onset of the wake at small Reynolds number which has not been described in the literature.

Experiments on a micropump based on the flow induced by a rotating cylinder inside a microchannel started fifteen years ago (Sen, Wajerski & Gad-el-Hak 1996) followed by a series of numerical simulations (Sharatchandra, Sen & Gad-el-Hak 1997, 1998; Decourtye, Sen & Gad-el-Hak 1998; Abdelgawad, Hassan & Esmail 2003). These experiments showed that, for a cylinder asymmetrically located in the channel, a global flow rate could be obtained with an average velocity of about 10 % of the cylinder surface velocity. Simulations were attempted to understand the effect of geometrical parameters such as relative size of the cylinder and the channel or eccentricity of the cylinder location, relative to the parabolic profile of the oncoming flow. Further simulations addressed the issue of a series of cylinders working as a multistage pump (Abdelgawad *et al.* 2005; Choi, Lee & Choi 2010). Theoretical approaches to the problem have been undertaken over the last decade through the lubrication theory (Day & Stone 2000; Matthews & Hill 2006). Nevertheless, in all these studies, the cylinder was rotating, not rolling on walls. In this context, the Stokes solutions have a limited validity because of the Stokes paradox (Matthews & Hill 2009). However, sometimes the Stokes solution can coincide with the Navier–Stokes solution even for small, compared to 1, but not zero Reynolds number. For example, the cusped corner was solved by Schubert in two particular cases: the cylinder spinning at a fix point on a wall and the non-rotating cylinder sliding on a wall (Schubert 1967).

Leaving aside the micropump problem and these two particular cases, the general flow of a rotating cylinder in the vicinity of a wall at low but non-zero Reynolds number has not been treated in the literature, unlike the corresponding high-Reynolds-number flow (Bhattacharyya, Mahapatra & Smith 2004; Stewart *et al.* 2010). The present paper fills that gap (§ 2) and clarifies the case of the Stokes flow (zero Reynolds number) that was tackled incompletely by different authors with sometimes contradictory results (Jeffery 1922; Schubert 1967; Wakiya 1975; Jeffrey & Onishi 1981).

In the literature, there are two distinct traditions for solving the Stokes flow around a cylinder rolling and translating in the vicinity of a wall. The oldest one, initiated by Jeffery (1922), used bipolar coordinates to solve the biharmonic equation around different configurations involving cylinders. The solution is obtained formally from a functional basis and the development is finite for a few particular cases. In general, the condition of finite velocity at infinity is not fulfilled, limiting the solution to flow confined between two eccentric cylinders with no contact point. Nevertheless the case of an external cylinder with an infinite radius can be treated at least to determine the forces and torque on the cylinder which only depend on the lowest coefficients in the development of the formal solution. While Jeffery only gave the torque around a cylinder spinning without contact near a fixed wall, Wakiya (1975) tried to solve the general problem with translation and rotation but without contact. He gave the force and the torque. Jeffrey & Onishi (1981) solved the same problem but only with translation or rotation of the cylinder. All these authors concluded that the lift was zero, the drag only depended on the translation velocity and the torque on the rotation velocity. Moreover, any non-zero component was found to tend towards infinity when the gap between the cylinder and the wall vanished. A discrepancy remained between

the drags given by Wakiya and Jeffrey although Jeffrey's expression coincided with a lubrication approach to the flow in the gap (Jeffrey & Onishi 1981). Beside these papers, Schubert (1967) solved the same cases as Jeffrey but with a totally different approach based on a transformation of the complex plane. The Schubert paper, more related to the problem of the cusp corner in the tradition of the paper of Moffatt (1964) on the sharp corner, did not provide expressions for the forces and torque but treated exclusively the flow without an interstice between the cylinder and the wall.

In contrast with these papers, the present research treats all the configurations of rotation and translation with and without a gap for Stokes flows and for small but non-zero Reynolds numbers. The discussion is concerned with forces, torque and the flow patterns and allows a better understanding of the contact point problem, drawing conclusions valid for high Reynolds number (§ 3). Analytical expressions of forces and torque (§ 3.3) also provided a good understanding of the physical origin of each component of force and torque and their distribution between the cylinder and the wall. A global effect of the gap is derived allowing its implementation in two-dimensional codes in order to avoid a detailed computation of the flow in the interstice.

The analysis of the forces exerted on the cylinder (§§ 2.4 and 3.3) established the unconditional presence of an interstice between the cylinder and the wall, leading to a lubrication situation very similar to the Taylor problem between two eccentric rotating cylinders (Taylor 1963). On one hand, the present paper (§§ 3.1 and 3.2) can be considered as an extension of Taylor's, if we consider the radius of the external cylinder as infinite. On the other hand, it is a generalization since Taylor limited his analysis to cylinders with the same surface velocity or with one rotating and one fixed. In addition, stream functions are determined (§ 3.4) whereas Taylor only solved the lubrication equation for pressure. The resolution of the velocity field in the interstice allows one to locate stationary saddle points where the fluid driven by the wall and that by the cylinder converge. In this region, the flow also splits into two parts: one passes through the interstice and one is pushed away from it and then flows around the cylinder before joining the interstice downstream.

Obviously the onset of a cavitation problem (§ 3.5) inside the interstice has been tackled by Taylor. In the present paper, the same logical development has been carried out, but, thanks to the knowledge of the velocity field, it was possible to demonstrate that cavitation induces three-dimensionality in agreement with the experiments by Taylor (1963) and Seddon & Mullin (2006).

Finally, the present computations at low Reynolds number fill the gap between the Stokes flow and literature results, particularly those of Stewart *et al.* (2010). Details are given on the formation process of the two-dimensional wake from an original vortex structure, already developed in a Stokes flow for prograde rolling.

2. Cylinder in contact with the wall

2.1. *Stokes analytical solution*

We consider the two-dimensional incompressible flow around a cylinder of radius R in contact at point O with a plane wall (figure 1). The kinematic viscosity of the fluid is ν. The cylinder translates with speed $U \geqslant 0$ parallel to the wall taken as x-axis. The rotation velocity of the cylinder is $\Omega = -kU/R$ where k is an algebraical dimensionless parameter, positive if the cylinder is rolling in the clockwise direction. We assume that the Reynolds number $Re = 2UR/\nu$ is very small compared to 1 and that the flow is governed by the Stokes equation. With the notation of figure 1 and in the frame of reference (Oxy) linked to the cylinder, stream function ψ satisfies the

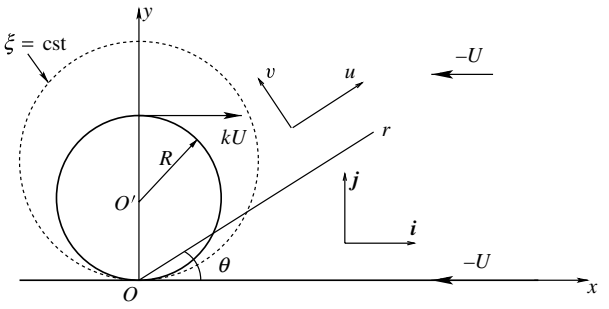

FIGURE 1. Notation: r, θ are the polar coordinates; R is the radius of the cylinder; $-U$ the upstream velocity ($U > 0$); O the origin of the frame of reference and the contact point. O' is the axis of the cylinder, u and v the polar components of the fluid velocity, k the ratio between the linear velocity on the cylinder surface and U; ξ is the dimensionless coordinate given by (2.14). Unit vectors $\boldsymbol{i}, \boldsymbol{j}$ and $\boldsymbol{k} = \boldsymbol{i} \wedge \boldsymbol{j}$ are the classical Cartesian basis.

biharmonic equation: $\Delta\Delta\psi = 0$. with the following boundary conditions, expressed in polar coordinates:

$$\frac{1}{r}\frac{\partial \psi}{\partial \theta} = -U \quad \text{for } \theta = 0 \tag{2.1a}$$

$$\frac{1}{r}\frac{\partial \psi}{\partial \theta} = -Uk\cos\theta \quad \text{for } r = 2R\sin\theta \tag{2.1b}$$

$$\frac{\partial \psi}{\partial r} = Uk\sin\theta \quad \text{for } r = 2R\sin\theta \tag{2.1c}$$

$$\frac{\partial \psi}{\partial r} = 0 \quad \text{for } \theta = 0 \tag{2.1d}$$

and at infinity:

$$\frac{1}{r}\frac{\partial \psi}{\partial \theta} = -U\cos\theta \quad \text{for } r \to \infty \tag{2.2a}$$

$$\frac{\partial \psi}{\partial r} = -U\sin\theta \quad \text{for } r \to \infty. \tag{2.2b}$$

Let us call

$$u = \frac{1}{r}\frac{\partial \psi}{\partial \theta} \quad \text{the radial component of the velocity} \tag{2.3a}$$

$$v = -\frac{\partial \psi}{\partial r} \quad \text{the orthoradial component.} \tag{2.3b}$$

Assuming that $\psi = 0$ on the wall $\theta = 0$ and on the cylinder $r = 2R\sin\theta$, the solution can be sought in the form $\psi = \sin\theta(r - 2R\sin\theta)F(r, \theta)$ where $F(r, \theta)$ is a function to be determined. In polar coordinates, a solution of the biharmonic equation can be

$$\psi(r, \theta) = \sum_{i=-1}^{1} f_i(\theta) r^i \tag{2.4}$$

where

$$f_{-1} = A_{-1}\cos\theta - B_{-1}\sin\theta + C_{-1}\cos 3\theta - D_{-1}\sin 3\theta, \tag{2.5}$$

$$f_0 = A_0 \cos 2\theta + B_0 \sin 2\theta + C_0\theta + D_0 \tag{2.6}$$

$$f_1 = A_1 \cos 2\theta + B_1 \sin 2\theta + C_1\theta \cos\theta + D_1\theta \sin\theta. \tag{2.7}$$

This expression induces a finite velocity at infinity, as required, and allows an easy identification with the form suggested above leading to

$$\psi = \frac{\sin\theta}{r}\left[r^2 B_1 - 2A_0 \sin\theta r + 4R(A_0 - RB_1)\sin^2\theta\right] \tag{2.8}$$

with only two undetermined constants that are fixed by the boundary conditions (2.1*a*) and (2.1*c*) to the following values: $B_1 = -U$ and $A_0 = -(2+k)UR$. Finally, the solution becomes

$$\psi = -\frac{U\sin\theta}{r}(r - 2R\sin\theta)\,[r - 2(1+k)R\sin\theta] \tag{2.9}$$

and the velocity components are

$$u = \frac{1}{r}\frac{\partial\psi}{\partial\theta} = -U\cos\theta\left[1 - 4(2+k)\frac{R\sin\theta}{r} + 12(k+1)\frac{R^2\sin^2\theta}{r^2}\right] \tag{2.10}$$

$$v = -\frac{\partial\psi}{\partial r} = U\sin\theta\left[1 - 4(k+1)\frac{R^2\sin^2\theta}{r^2}\right]. \tag{2.11}$$

It is interesting to separate the effect of the translation and the rotation. Let us call $V = kU = \Omega/R$ the linear velocity on the surface of the cylinder. Stream function ψ becomes

$$\psi = -\frac{U\sin\theta}{r}(r - 2R\sin\theta)^2 + \frac{2RV\sin^2\theta}{r}(r - 2R\sin\theta). \tag{2.12}$$

Case $U = 0$ (no translation), corresponds to a cylinder spinning over a fixed point O on a steady plate and was obtained by Schubert (1967) in the form $\psi = 2RV(y^2/r^2)[1 - 2R(y/r^2)]$ with $y = r\sin\theta$. Figure 2 depicts the corresponding streamlines that Schubert could not plot in 1967. The cylinder squeezes the fluid in the vicinity of the rotating surface inducing a global flow rate Q_S (from right to left in the figure). According to (2.12) for $U = 0$, this global flow rate is $Q_S = 2RV$ since $0 \leqslant \psi \leqslant 2RV$. This is a limit case of a Sen micropump (Sen *et al.* 1996) with a cylinder radius which is very small compared to the channel height and without a gap between the cylinder and the adjacent wall.

Case $k = 0$ or $V = 0$ corresponds to a cylinder sliding on a plate at a constant velocity U without rotation. The stream function was also obtained but not plotted by Schubert (1967) in the form $\psi = -Uy[1 - (Ry/r^2)]^2$. The flow pattern is shown on figure 3(*e*).

Formula (2.12) appears to be nothing but the superposition of the two Schubert flows as expected by the superposition principle applied to the present linear problem.

Another comparison with the literature is possible by extracting an approximation of ψ in the vicinity of O where $\sin\theta \approx y/x$ and $r \approx x$. This asymptotic form is

$$\psi_O \approx U\left(4R^2(k+1)\frac{y^3}{x^4} - 2R(k+2)\frac{y^2}{x^2} + y\right) \tag{2.13}$$

which is a generalization of the equation obtained by Bhattacharyya *et al.* (2004) for $k = 1$, $U = R = 1$.

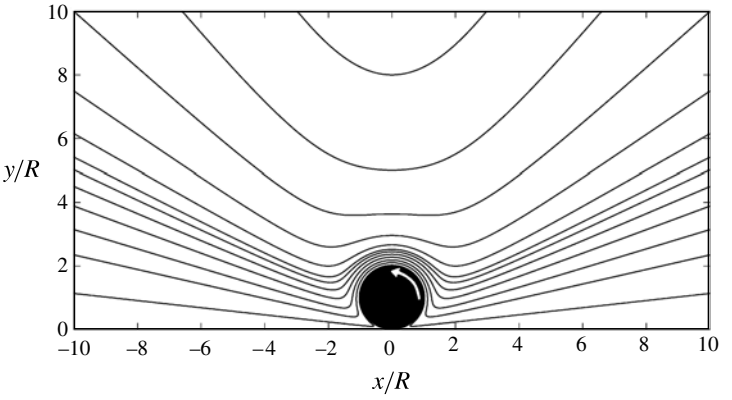

FIGURE 2. Streamlines of the Stokes flow around cylinder spinning at a fixed point for $V = 1$ and $R = 1$.

Before turning to a detailed discussion about the flow, let us introduce the useful change of variable:

$$\xi = \frac{r}{2R\sin\theta}. \tag{2.14}$$

Notice that curves $\xi = \text{const.}$ are circles of diameter $2\xi R$, tangent to the cylinder at point O, the cylinder is the circle $\xi = 1$ and the flow region is located where $\xi \geqslant 1$. The solution can be rewritten in dimensionless form as a function of ξ and θ:

$$\bar{\psi} = \frac{\psi}{UR} = -2\frac{\sin^2\theta}{\xi}[\xi - 1][\xi - (k+1)] \tag{2.15a}$$

$$\bar{u} = \frac{u}{U} = -\cos\theta\left[1 - \frac{2(k+2)}{\xi} + \frac{3(k+1)}{\xi^2}\right] \tag{2.15b}$$

$$\bar{v} = \frac{v}{U} = \sin\theta\left[1 - \frac{k+1}{\xi^2}\right]. \tag{2.15c}$$

2.2. *Flow patterns in the Stokes regime*

Figure 3 depicts the flow patterns for values of k between 2 and -2. The analytical solution given by (2.9) is compared with computational results calculated with the full incompressible two-dimensional Navier–Stokes equations at $Re = 2UR/\nu = 0.005$ (see the next section for details about the numerical method). These patterns have never been presented before in the literature, but can be compared qualitatively with some results of Ballal & Rivlin (1976) or Finn & Cox (2001) for the flow between two non-concentric cylinders.

It is easy to verify with (2.15*b*) that for $\sin\theta \neq 0$ and $\cos\theta \neq 0$ stagnation points only exist if $\xi = \pm\sqrt{k+1} = (k+2) \pm \sqrt{k^2+k+1}$, which only happens for $k = 0$ or $k = -1$, i.e. respectively $\xi = 1$ (the cylinder) and $\xi = 0$ (irrelevant physically here). This simply underlines a trivial situation since for $k = 0$ the cylinder is fixed (figure 3*e*). Furthermore, in all cases, the contact point O is also a double stagnation point, once for the upstream flow and once for the downstream flow, since for $\theta \to 0$ or $\theta \to \pi$, v is always equal to 0 whereas u is zero for a finite value of ξ: $\xi = (k+2) \pm \sqrt{k^2+k+1}$, which is only possible for these values of θ if r also tends towards 0.

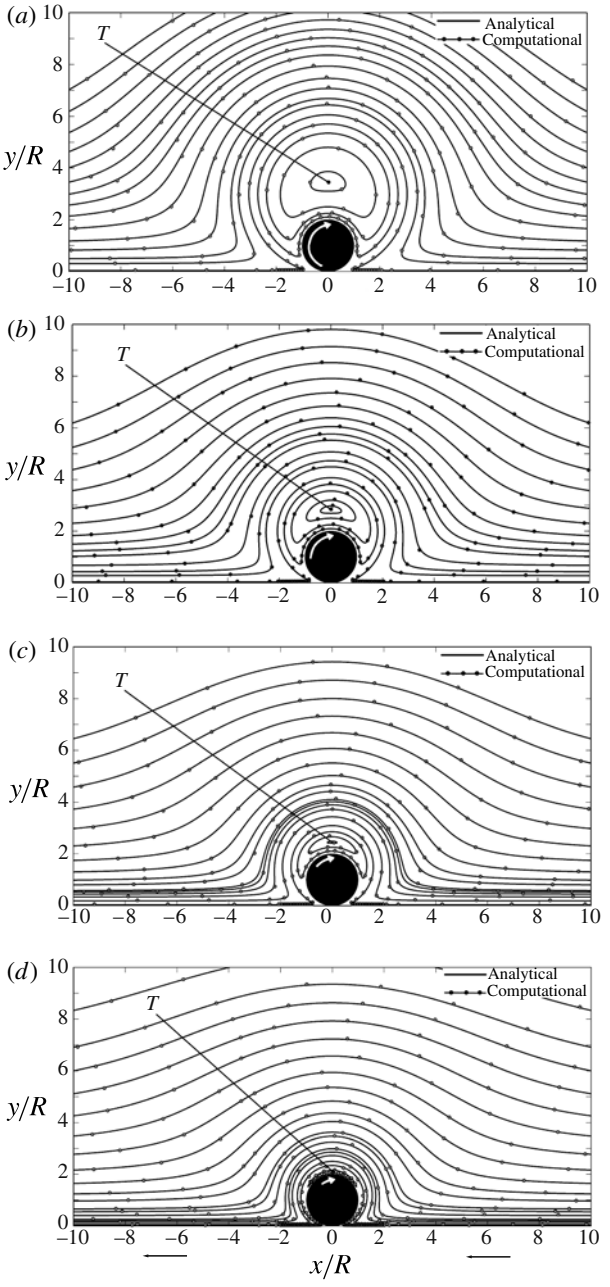

FIGURE 3. For caption see next page.

The most interesting feature is the existence of a stagnation point T at $\theta = \pi/2$ for $k > 0$ (figures 3*a–d*). For this value of θ, u is always zero whereas v is equal to 0 for $\xi = \sqrt{k+1}$, i.e. $y = 2R\sqrt{k+1}$. This point is clearly located inside the flow only if $k \geqslant 0$. Turning back to the stream function (2.15*b*), it can be seen that condition $k > 0$ determines the existence of a third branch of the streamline $\psi = 0$ given by $\xi = (k+1)$. This branch is a circle of radius $2(k+1)R$, tangent to Ox at point O

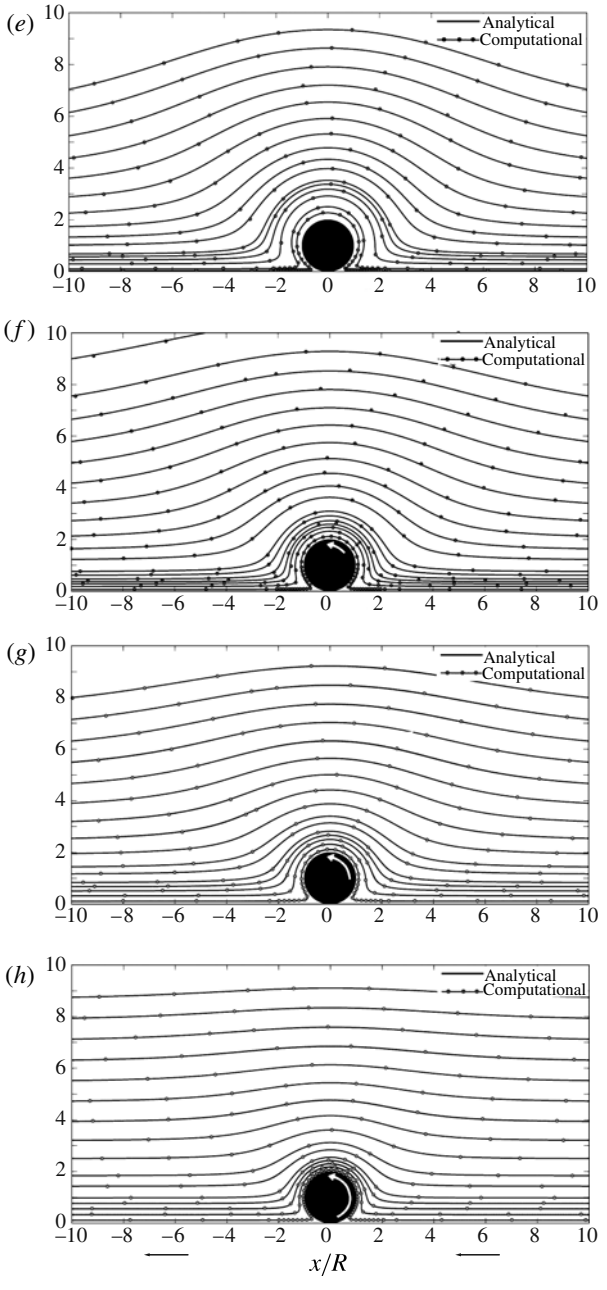

FIGURE 3. (cntd). Streamlines of the Stokes flows. Continuous lines are analytical streamlines ψ (2.9), dotted lines are numerical computations at $Re = 2UR/\nu = 0.005$. (*a–d*) Prograde rotation; (*e*) fixed cylinder; (*f–h*) retrograde rotation. (*a*) $k = 2$, the cylinder is sliding on the wall, a cylindrical vortex structure of radius $3R$ is generated by the rotation, point T is located at $y = 2R\sqrt{3}$; (*b*) $k = 1$, the cylinder is rolling without slip, the vortex radius is reduced to $2R$, point T is located at $y = 2R\sqrt{2}$; (*c*) $k = 0.5$, the vortex radius is reduced to $1.5R$; (*d*) $k = 0.1$, the vortex is vanishing; (*e*) $k = 0$, the cylinder is only sliding on the wall, first Schubert case (Schubert 1967), the vortex has disappeared; (*f–h*) $k = -0.5, -1, -2$ respectively, the vortex does not exist and the flow is progressively squeezed in the vicinity of the cylinder.

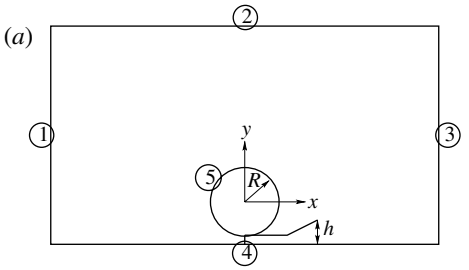

(b)

Boundary	Conditions
1	Outlet velocity U
2	Open boundary $p = 0$
3	Inlet velocity U
4	Moving wall, velocity U
5	Moving wall, velocity $k.\ U$

FIGURE 4. Numerical boundary conditions.

and centred on Oy. Between this branch and the cylinder ($\xi = 1$), the streamlines are closed loops and point T is the topological centre of this vortex structure. Surprisingly, this vortex protects the cylinder from any contact with the external flow. The stream function values then vary from zero on the cylinder, to $\psi_s = 2RU(\sqrt{k+1} - 1)^2$, the maximum value corresponding to a streamline reduced to point T. Between the vortex boundary ($\xi = k + 1$) and the wall, the stream function is negative. Such a vortex structure does not exist for $k \leqslant 0$ (figure 3*e–g*). In all cases, the symmetry ($x \to -x$) of the streamlines is a consequence of the Stokes regime reversibility.

2.3. *Numerical simulations at low Reynolds numbers*

Numerical simulations were carried out with the commercial finite-element method (FEM) program Comsol 3.4 (FEMLAB) on a 4-core processor and 20 GB RAM computer. The model was solved using the two-dimensional laminar Navier–Stokes flow module. Simulations were made with a perfect contact at point O and with different gaps between the cylinder and the wall. The lift, drag and torque on the cylinder or at point O were extracted for each configuration.

In order to cover the range between the Stokes flow conditions and the beginning of the first instability of the wake that happens around $Re = 80$ (Stewart *et al.* 2010), the Reynolds number was varied between $Re = 0.005$ and $Re = 60$. According to the value of k and Re, the boundaries were located at least at 60 times the radius R in order to remove any influence of the size of the computational domain. Tests were made to minimize the influence of this size and optimize the mesh resolution. The boundary conditions are summarized in figure 4.

The meshes were similar for every configuration, with 400 elements around the cylinder and with a maximum height s of the elements in the far field such that $s/R = 0.5$. Figure 5 shows an example of a mesh, the coarse mesh for clarity. Structured triangular elements were selected because they were more adapted to a smooth representation of the cylinder surface. Although a fast convergence in pressure and in the velocity values was observed with coarse meshes, a higher level of refinement was necessary to control the mesh quality near the nip and for a good determination of the forces and torque applied on the cylinder. The typical number of elements was approximately 70 000.

Our computations can also be compared with the very few papers published on the subject. In Stewart *et al.* (2006, 2010) for Reynolds numbers $Re = 2UR/\nu$ from 20 to 500, contrary to the Stokes solution, a wake is observed inducing an asymmetry between the upstream and downstream flows. A transition between steady and unsteady wakes appears at $Re \approx 80$. Nevertheless, surprisingly, in Bhattacharyya *et al.* (2004) numerical results, computed for $Re = 100$, are symmetrical and similar

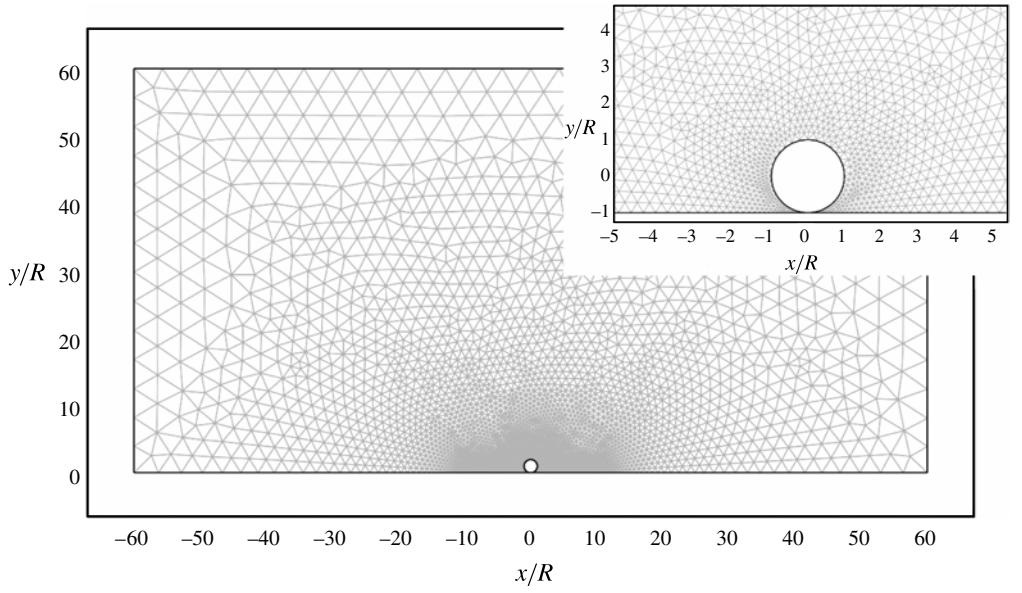

FIGURE 5. Example of a mesh (7002 elements) chosen coarser than in the computation for clarity.

to our Stokes solution. This is probably due to a very dissipative and highly viscous computational scheme. In our computations, taking $k = 1$ as example, the increase of Re from 0.01 to 1 displaces the vortex structure downstream, resulting in an emerging wake (figure 6*a*). The topological centre T of this structure could be relocated on the former symmetry plane $x = 0$ by considerably increasing the rotation velocity ($k = 6$) but the vortex structure remained asymmetrical (figure 6*b*). For $Re = 60$ and boundaries at $x/R = \pm 100$ and $y/R = 100$ our computation gives the same result as Stewart *et al.* (2010) with a second vortex structure of centre T' trapped between the wall and the first vortex (figure 6*c*). For $k = 1$, the transition from one vortex to two vortices in the wake appears for $35 < Re < 40$ as shown in figure 7. It must be underlined that streamlines displayed here are computed without an interstice between the cylinder and the wall but does not differ from those computed with a gap of height h provided that $h/R \ll 1$. This indicates that the contact area has no influence on the far flow field. This result is confirmed theoretically in the next section, nevertheless it will be shown that the interstice plays a prominent role in the forces and torque applied on the cylinder.

2.4. *Stresses, forces and torque in the Stokes regime for a perfect contact*

The pressure field is a solution of $\nabla p = \mu \Delta \boldsymbol{V}$ where $\mu = \rho\nu$ is the viscosity and $\boldsymbol{V}$ the flow velocity field. Using (2.10) and (2.11), the integration gives

$$p(r,\theta) = 8\mu R \cos\theta \frac{U}{r^2}\left[(k+2)\sin\theta + \frac{R}{r}(k+1) - 4\frac{R}{r}(k+1)\sin^2\theta\right] + p_\infty. \quad (2.16)$$

The pressure repartition on the cylinder, $r = 2R\sin\theta$, is

$$p_c = \mu \frac{\cos\theta}{\sin^3\theta}\frac{U}{R}\left[(k+1) - 2k\sin^2\theta\right] + p_\infty. \quad (2.17)$$

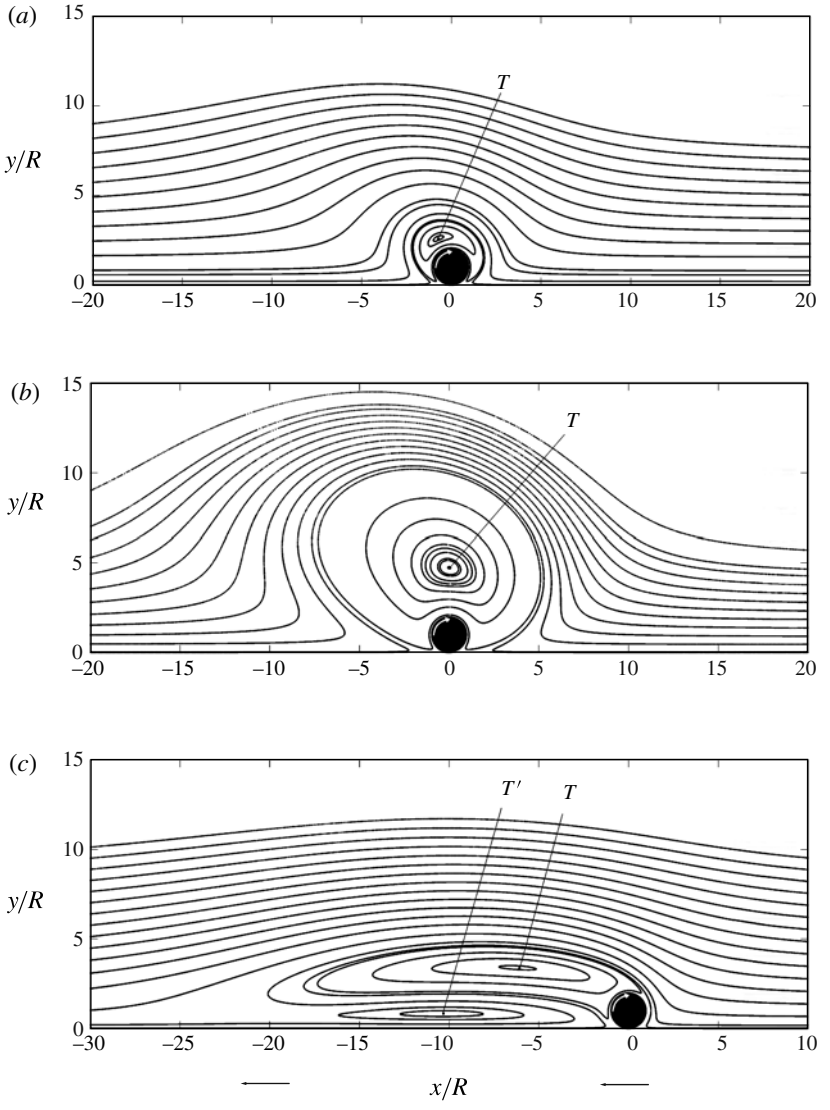

FIGURE 6. Streamlines for low but not zero Reynolds numbers without interstice. (*a*) Rolling cylinder with no-slip condition ($k = 1$) at $Re = 1$. (*b*) Rotation velocity increased to $k = 6$ for $Re = 1$: the topological centre T of the vortex structure is relocated on the Oy axis but the vortex remains asymmetrical. (*c*) Flow for $k = 1$ and $Re = 60$: the vortex structure becomes a wake and induces a second vortex of centre T' near the wall. This result coincides with the computation of Stewart *et al.* (2010), but is more detailed.

As a consequence, $p_c \to \infty$ when $\theta = 0$ and $p_c \to -\infty$ when $\theta = \pi$. Therefore, just downstream of the contact point O, the pressure has no physical meaning unless the reference p_∞ is infinite. The same conclusion can be deduced from the pressure on the wall ($\theta = 0$)

$$p_w = \frac{8\mu U R^2 (k+1)}{x^3} + p_\infty. \tag{2.18}$$

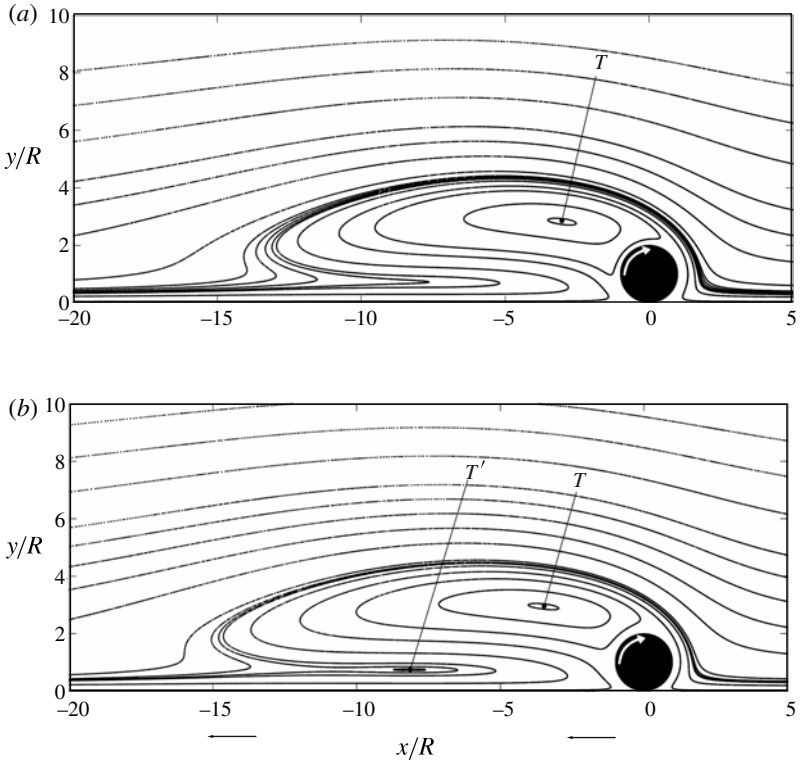

FIGURE 7. Streamlines for $k = 1$: (*a*) $Re = 35$, (*b*) $Re = 40$, without interstice. The transition from one vortex to two vortices in the wake happens when the flow driven by the wall and that driven upstream by the vortex annihilate each other. As a consequence, a new point T' where $u = 0$ and a closed streamline is generated.

The agreement between the Stokes solution and the numerical computations at low but non-zero Reynolds number underlines the fact that this infinite pressure is not specific to the Stokes solution but to the incompressible Navier–Stokes equations. Actually, incompressible Navier–Stokes solutions are always independent of the reference pressure. For a finite value of p_∞, it is not possible to avoid an infinitely negative pressure except by introducing a compressible effect or, in the case of liquids, cavitation. Compressible effects were underlined by Chauveau (2002) in computations on an F1 racing car wheel. For liquids, the cavitation in narrow channels is well known and was particularly well studied in Taylor (1963), and others (Savage 1982; Coyle, Macosko & Scriven 1986) but with different geometries and boundary conditions. More recently, cavitation was reported in Seddon & Mullin (2006) by careful experiments on a rolling cylinder in the Stokes regime. According to (2.17) or (2.18), cavitation bubbles must appear downstream for $k > -1$ but also upstream if $k < -1$, i.e. for a retrograde rolling inducing a surface velocity on the cylinder higher than the translation one. All this means that there are no realistic fully incompressible Navier–Stokes solutions to the problem of a cylinder rolling or sliding on a wall with a perfect contact. Nevertheless, it is worthwhile deriving the viscous stresses in order to check that there is no compensation between pressure and normal viscous stresses and obtain the forces and torque on the cylinder and the wall in the case of a perfect contact.

The viscous stresses are calculated from the viscous tensor $\boldsymbol{\sigma}_{visc} = 2\mu \boldsymbol{D}$ where $\boldsymbol{D}$ is the stain rate tensor. Using again (2.10) and (2.11), the derivation gives

$$\boldsymbol{\sigma}_{visc}(r,\theta) = 4\mu U \frac{R}{r^2}\left[(2+k) - 6(k+1)\frac{R}{r}\sin\theta\right]\begin{pmatrix} -\sin 2\theta & \cos 2\theta \\ \cos 2\theta & \sin 2\theta \end{pmatrix} \tag{2.19}$$

which becomes on the cylinder ($r = 2R\sin\theta$):

$$\boldsymbol{\sigma}^c_{visc} = \frac{\mu U(2k+1)}{R\sin^2\theta}\begin{pmatrix} \sin 2\theta & -\cos 2\theta \\ -\cos 2\theta & -\sin 2\theta \end{pmatrix} \tag{2.20}$$

and on the wall ($\theta = 0$ and π):

$$\boldsymbol{\sigma}^w_{visc} = \frac{4\mu UR(2+k)}{x^2}\begin{pmatrix} 0 & 1 \\ 1 & 0 \end{pmatrix}. \tag{2.21}$$

providing a pure shear stress: $T_w = (4\mu UR(2+k))/x^2$.

For $k \geqslant 0$, it is also interesting to evaluate the stress tensor on the vortex boundary ($r = 2R(k+1)\sin\theta$):

$$\boldsymbol{\sigma}^v_{visc} = \frac{\mu U(1-k)}{(k+1)^2 R\sin^2\theta}\begin{pmatrix} \sin 2\theta & -\cos 2\theta \\ -\cos 2\theta & -\sin 2\theta \end{pmatrix} \tag{2.22}$$

which shows that for a non-slipping cylinder ($k = 1$), the vortex boundary is not subjected to any shear stresses.

The lift and drag forces are obtained by projecting stresses on the x- and y-axes and integrating along the cylinder surface. We have

$$T_x = \boldsymbol{i}\cdot\boldsymbol{\sigma}^c_{visc}\cdot\boldsymbol{n} = \frac{\mu U(2k+1)}{R\sin^2\theta}\cos 2\theta \tag{2.23}$$

and

$$T_y = \boldsymbol{j}\boldsymbol{\sigma}^c_{visc}\cdot\boldsymbol{n} = \frac{\mu U(2k+1)}{R\sin^2\theta}\sin 2\theta. \tag{2.24}$$

When θ is replaced by $\pi - \theta$, T_y and p_c (2.17) are antisymmetric, and therefore, the lift F_y is zero. Note that, mathematically, the pressure lift is given by:

$$\lim_{\epsilon\to 0}\int_{\epsilon}^{\pi-\epsilon} \mu\frac{\cos\theta}{\sin^3\theta}\frac{U}{R}\left[(k+1) - 2k\sin^2\theta\right]\cos 2\theta(2R)\,\mathrm{d}\theta \tag{2.25}$$

which converges to zero only in the Cauchy principal value.

On the contrary, the global drag

$$\boldsymbol{D}_c = \int_0^{\pi}(T_x - (p_c - p_\infty)\sin 2\theta)\,(2R\,\mathrm{d}\theta)\boldsymbol{i} = -2\mu U\int_0^{\pi}\frac{\mathrm{d}\theta}{\sin^2\theta}\boldsymbol{i} \tag{2.26}$$

diverges to $-\infty$ except if $U = 0$ where it is zero. Note that $\boldsymbol{D}_c$ is independent of k.

The same happens for the torque applied by the fluid on the cylinder:

$$\mathscr{M}_{c/O'} = 2(2k+1)\mu UR\int_0^{\pi}\frac{\mathrm{d}\theta}{\sin^2\theta}. \tag{2.27}$$

The only global quantity that gives a finite value is the viscous torque on the cylinder at the contact point O. We have

$$\mathscr{M}_{v/O} = \int_0^{\pi} (2R\sin\theta)\frac{(2k+1)\mu U}{R\sin^2\theta}\sin\theta(2R)\,\mathrm{d}\theta = 4\pi(2k+1)\mu UR. \tag{2.28}$$

On the wall, the drag is

$$\boldsymbol{D}_w = \int_{-\infty}^{\infty} T_w\,\mathrm{d}x\,\boldsymbol{i} = 4U\mu(k+2)R\int_{-\infty}^{\infty}\frac{1}{x^2}\,\mathrm{d}x\,\boldsymbol{i} \tag{2.29}$$

and the torque at point O is

$$\mathscr{M}_w = -\int_{-\infty}^{\infty} xp_w\,\mathrm{d}x = -8\mu U(k+1)R^2\int_{-\infty}^{\infty}\frac{1}{x^2}\,\mathrm{d}x. \tag{2.30}$$

Note that the change of variable $x/R = \tan\theta$ leads to $I = R\int_{-\infty}^{\infty}\mathrm{d}x/x^2 = \int_0^{\pi}\mathrm{d}\theta/\sin^2\theta$. Despite the fact that I is infinite, the forces and torque can be written formally:

$$\boldsymbol{D}_c = -2\mu UI\,\boldsymbol{i}, \quad \mathscr{M}_{c/O'} = 2(2k+1)\mu URI \tag{2.31}$$

$$\boldsymbol{D}_w = 4U\mu(k+2)I\,\boldsymbol{i}, \quad \mathscr{M}_w = -8\mu U(k+1)RI. \tag{2.32}$$

These expressions clearly show that the global balance of forces and torque is not fulfilled. It is therefore necessary to introduce a point force and torque exerted by the fluid at point O:

$$\boldsymbol{D}_O = -(\boldsymbol{D}+\boldsymbol{D}_w) = -2(2k+3)\mu UI\,\boldsymbol{i}, \quad \mathscr{M}_O = 4(k+1)\mu URI. \tag{2.33}$$

Unfortunately at this stage it is impossible to distinguish which part of D_O and $\mathscr{M}_O$ is applied on the cylinder and on the wall.

It is clear now that cavitation or compressibility will substantially change the lift and drag forces. For example, if a cavitation bubble appears just downstream of the contact point O, where p drops towards zero, the antisymmetry is broken and an infinite positive lift appears since the integral in (2.25) does not converge any more. It is therefore impossible to maintain the cylinder in contact with the wall. A very tiny flow must pass under the cylinder and, in two dimensions, this must be represented by an interstice between the wall and the cylinder. In real three-dimensional situations, the roughness of the surfaces even at molecular level is compatible with both the wall–cylinder contact and a non-zero interstitial flow, but that will not modify the solution of the Navier–Stokes equations far enough from the contact area and the onset of cavitation for a finite value of p_∞.

3. Interstitial flow between the cylinder and the wall

3.1. *Lubrication solution*

In two dimensions, a more realistic treatment of the problem must therefore take into account a gap between the cylinder and the wall. The direct treatment by bipolar coordinates (Jeffery 1922) is limited to Stokes flows around the cylinder whereas the lubrication approach to the interstitial flow is valid for any Reynolds number provided that $Re\,h^2/R^2 \ll 1$ where h is the characteristic height of the interstice, here the minimum distance between the wall and the cylinder. Moreover, the lubrication equation is an easy way to determine the pressure field and discuss the cavitation onset, while the bipolar approach generally provides the pressure field by means of an infinite formal sum of undetermined coefficients. For these reasons, the lubrication

point of view was adopted here. In fact, the problem is a generalization of the one dealt with in Taylor (1963) for $k = 0$ and 1 and the approach presents similarities with Coyle *et al.* (1986) treating counter- and corotating cylinders. However, all published papers related to coating processes between cylinders and with a gas–liquid interface.

The fluid flows between the wall ($y = 0$) and the cylinder, locally approximated by $y_c = h + (x^2/2R)$. Calling u_x and v_y the velocity components along the Ox- and Oy-axes, the problem is reduced to

$$\frac{1}{\mu}\frac{\partial p}{\partial x} = \frac{\partial^2 u_x}{\partial y^2} = \frac{A(x)}{\mu} \quad \text{for } x \ll R \tag{3.1}$$

with the following boundary conditions:

$$u_x = -kU \quad \text{for } y = y_c \tag{3.2a}$$

$$u_x = -U \quad \text{for } y = 0. \tag{3.2b}$$

The solution for u_x, as a function of the pressure gradient, is:

$$u_x = \frac{A(x)}{2\mu}\left(y - \frac{x^2}{2R} - h\right)y + \frac{(1-k)Uy}{h + \dfrac{x^2}{2R}} - U. \tag{3.3}$$

The second component of the velocity v_y is obtained by integrating the mass conservation equation:

$$v_y = -\int_0^y \frac{\partial u_x}{\partial x}\,\mathrm{d}\hat{y} \tag{3.4}$$

that results in:

$$v_y = \left[\frac{(1-k)Ux}{2R\left(h + \dfrac{x^2}{2R}\right)^2} + \frac{Ax}{4\mu R} - \frac{A'}{2\mu}\left(\frac{y}{3} - \frac{x^2}{4R} - \frac{h}{2}\right)\right]y^2. \tag{3.5}$$

It is useful to rewrite the solution in terms of the algebraic mass flux: $Q = \int_0^{y_c} u_x\,\mathrm{d}y$, which gives for the pressure gradient

$$A = -\frac{12\mu Q}{y_c^3} - \frac{6U(k+1)\mu}{y_c^2} \tag{3.6}$$

and, for the velocity field:

$$\frac{u_x}{U} = -3Y^2(2q + k + 1) + 2Y(3q + k + 2) - 1 \tag{3.7}$$

$$\frac{v_y}{U} = \frac{Y^2 x}{R}((6q + k + 2) - 2Y(3q + k + 1)) \tag{3.8}$$

where $Y = y/y_c$ and $q(x/R) = Q/Uy_c$.

Given that $\mathrm{d}y = y_c\,\mathrm{d}Y + Y(x/R)\,\mathrm{d}x$, it is easy to deduce by integration of (3.7) and (3.8), that the stream function is

$$\Psi = Uy_c\left[-(2q + k + 1)Y^3 + (3q + k + 2)Y^2 - Y\right]. \tag{3.9}$$

The dimensionless solution $\bar{\Psi} = \Psi/Uh$ only depends on parameters $q^* = Q/Uh$ and h/R.

3.2. *Problem closure for a completely flooded interstice*

The present lubrication solution can be considered as focusing on the flow in the vicinity of point O (figure 1) when the contact is not perfect. It is worthwhile verifying that it is asymptotically compatible with the Stokes solution far from O. Taking the velocity components (2.15*b*) and projecting it on the x and y directions gives

$$\frac{u_x}{U} = -(3\cos^2\theta - \sin^2\theta)\frac{1}{\xi^2}(k+1) + 2\cos^2\theta\frac{1}{\xi}(k+2) - 1 \tag{3.10}$$

$$\frac{v_y}{U} = 2\sin\theta\cos\theta\left(\frac{1}{\xi}(k+2) - 2\frac{1}{\xi^2}(k+1)\right). \tag{3.11}$$

The interstitial area is characterized by $\theta \ll 1$ and its asymptotic border by $x \to \infty$, which leads to

$$Y \approx \frac{1}{\xi} \approx \frac{2Ry}{x^2} \ll 1, \quad \sin\theta \approx \frac{y}{x}, \quad \cos\theta \approx 1. \tag{3.12}$$

With this approximation, Stokes solutions (3.10) and (3.11) become

$$\frac{u_x}{U} = -3Y^2(k+1) + 2Y(k+2) - 1 \tag{3.13}$$

$$\frac{v_y}{U} = \frac{Y^2 x}{R}((k+2) - 2Y(k+1)), \tag{3.14}$$

that is, exactly (3.7) and (3.8) if $q \longrightarrow 0$, which is the case when $x^2/2Rh \gg 1$.

This shows that, as suggested by the numerical computations, far enough from the contact area, the global Stokes flows either with a perfect contact or with a gap between the wall and the cylinder, are identical. Unfortunately this does not help to determine flux Q in this gap. However, this can be done analytically as long as the interstitial flow is governed by Rayleigh equation (i.e. $Re\, h^2/R^2u \ll 1$) and is completely flooded (no cavitation). In fact, in that case, pressure gradient $A(x)$ (3.6) is an even function of x and, therefore, $p - p_\infty$ must be odd. At $x = 0$, let us write

$$p(0) - p_\infty = \int_{-\infty}^{0} A\,\mathrm{d}x = 0 \tag{3.15}$$

and introduce, for convenience, the following notation:

$$q^* = \frac{Q}{Uh}; \quad Z = \frac{q}{q^*} = \frac{h}{y_c} = \left(1 + \frac{x^2}{2Rh}\right)^{-1}, \quad |x| = \sqrt{2Rh}\sqrt{\frac{1-Z}{Z}}. \tag{3.16}$$

Equation (3.15) becomes

$$\int_0^1 \frac{q^* Z^{3/2} + \dfrac{k+1}{2}Z^{1/2}}{\sqrt{1-Z}}\,\mathrm{d}Z = 0 \tag{3.17}$$

and therefore

$$q^* = -\frac{k+1}{2}\frac{\displaystyle\int_0^1 \frac{Z^{1/2}}{\sqrt{1-Z}}\,\mathrm{d}Z}{\displaystyle\int_0^1 \frac{q^* Z^{3/2}}{\sqrt{1-Z}}\,\mathrm{d}Z} = -\frac{k+1}{2}\frac{\pi/2}{3\pi/8} = -\frac{2}{3}(k+1). \tag{3.18}$$

The explicit expression of p is therefore

$$p - p_\infty = \mathrm{sgn}(x)\frac{12\mu U}{h^2}\sqrt{\frac{Rh}{2}}(k+1)\int_0^Z \frac{\sqrt{z}(-2z/3+1/2)}{\sqrt{1-z}}\,\mathrm{d}z. \tag{3.19}$$

Integration and going back to the original variables gives

$$p - p_\infty = \frac{2\mu U(k+1)}{h^2}\frac{x}{\left(1+\dfrac{x^2}{2Rh}\right)^2}. \tag{3.20}$$

This expression tends towards the pressure distribution on the wall (2.18) for the Stokes flow with perfect contact if $x^2/2Rh \gg 1$. Distance $\sqrt{2Rh}$ appears to be the characteristic length of the interstitial area along the x axis and also corresponds to points $\pm x_{A'}$ where the derivative A' of the pressure gradient is zero. This can be verified easily since, according to (3.6), $A' = 0$ for $q(x_{A'}) = q^*h/y_c = -(k+1)/3$. This is understandable from a physical point of view: in the case of a perfect contact, the pressure gradient increases continuously until point O, but when the interstice exists, it stops growing at a certain distance because of the leak under the cylinder. This distance $x_{A'}$ can therefore be considered as the characteristic distance of influence of the interstice. It is remarkable that $x_{A'}$ do not depend on k, and that $x_{A'}/h = \sqrt{2R/h}$ is just a geometrical factor. This result is valid as long as the Rayleigh equations are also valid and the interstice is completely flooded, which does not depend directly on the Reynolds number $Re = 2UR/\nu$ of the external flow. Therefore, the present results are applicable to high-Reynolds-number situations as in Stewart *et al.* (2010) if h is small enough.

3.3. *Forces and torque for Stokes flows*

Forces and torque exerted on the cylinder can be calculated from the global linear and angular momentum on the domain defined in figure 8. For the cylinder in Stokes regime this can be done analytically. From (2.19) and (2.16) it is easy to show that viscous and pressure forces decay at infinity like $1/r$ and that the contribution of the surface Σ to the viscous torque at O, $\int_0^\pi 4\mu U(2+k)\cos 2\theta\,\mathrm{d}\theta$ is zero by symmetry. On a finite numerical square domain, this is not strictly the case and therefore the numerical cylinder torque must be corrected by removing the residual torque generated by external boundaries.

Since the fluxes of linear and angular momentum are zero on the domain of figure 8, the forces and torque exerted on the cylinder are just balanced by those applied on the wall. It follows immediately, by the antisymmetry of the pressure at the wall, that no lift force is applied on the cylinder as long as the interstice is completely flooded and without cavitation effects. Therefore, the drag is the only force that balances the viscous stress on the wall. As the lubrication and the Stokes solution are identical on the wall far from the nip, the viscous stress can be deduced from (3.3):

$$\begin{aligned}\boldsymbol{D} &= -\int_{-\infty}^{\infty} \mu\left.\frac{\partial u_x}{\partial y}\right|_{y=0}\boldsymbol{i}\,\mathrm{d}x \\ &= 2\mu U\sqrt{\frac{2R}{h}}\left(k\int_{-\infty}^{\infty}\frac{\mathrm{d}X}{(1+X^2)^2} - (k+2)\int_{-\infty}^{\infty}\frac{X^2\,\mathrm{d}X}{(1+X^2)^2}\right)\boldsymbol{i}\end{aligned} \tag{3.21}$$

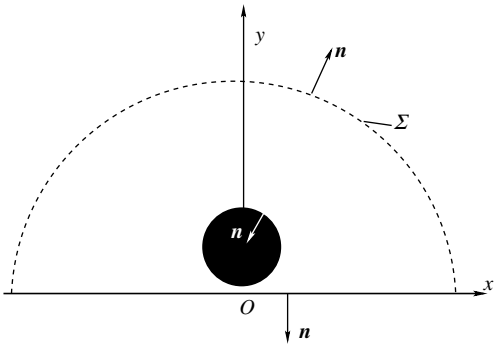

FIGURE 8. Integration domain for forces and torque. Surface Σ is a cylinder centred on point O with a radius tending toward infinity.

where $X = x/\sqrt{2Rh}$, resulting in

$$\boldsymbol{D} = -2\pi\mu U\sqrt{\frac{2R}{h}}\boldsymbol{i}. \tag{3.22}$$

Notice that this result surprisingly does not depend on k. This is because in (3.21) both integrals are equal although they have a different physical origin. Rewriting the viscous stress on the wall in dimensional form and assuming that $x^2/2Rh \gg 1$, we have

$$\mu\left.\frac{\partial u_x}{\partial y}\right|_{y=0} \approx \frac{8\mu UR^2}{x^4}(kh - (k+2)x^2), \tag{3.23}$$

which implies that the first contribution is negligible far from the nip and strictly zero for $h = 0$. The first integral in (3.21) is mainly the contribution of the interstice and the second one the influence of the rest of the wall. That is why, for the perfect contact problem, the contribution of the contact point could only be deduced from the global balance and the force obtained on the wall was only the second contribution. Comparing (3.22) and (2.29) shows that it is possible to model the interstice as a contact point, substituting $\pi/4\sqrt{2R/h}$ by I in (2.29) and assuming that a force of $\boldsymbol{F}_{Ow} = -\pi\mu Uk\sqrt{2R/h}\boldsymbol{i}$ is applied on the wall at point O. Within this model, it follows from (2.33) that point O applies on the cylinder a force $\boldsymbol{F}_{Oc} = -(3\pi/2)\mu U\sqrt{2R/h}\boldsymbol{i}$ resulting in the global drag (3.22) on the cylinder. Notice that drag $\boldsymbol{D}_c = -(\pi/2)\mu U\sqrt{2R/h}\boldsymbol{i}$ (2.26) is only a quarter of $\boldsymbol{D}$ and represents the contribution of the whole cylinder except the interstice.

As with the forces, in the Stokes regime the cylinder torque, with respect to point O, only balances the pressure torque applied on the wall. From (3.20) this can be written

$$\boldsymbol{M}_{/O} = \int_{-\infty}^{\infty} p_w x\,\mathrm{d}x\boldsymbol{k} = 4\mu U(k+1)R\sqrt{\frac{2R}{h}}\int_{-\infty}^{\infty}\frac{X^2}{(1+X^2)^2}\,\mathrm{d}X\boldsymbol{k} \tag{3.24}$$

and finally

$$\boldsymbol{M}_{/O} = 2\pi\mu U(k+1)R\sqrt{\frac{2R}{h}}\boldsymbol{k}. \tag{3.25}$$

Applying the same substitution of I, this is exactly the opposite of torque $\mathscr{M}_w$ (2.30), and from (2.33) we can deduce that a torque $\mathscr{M}_{cO} = \pi\mu U(k+1)\sqrt{2R/h}$ is applied on

the cylinder at point O. The torque at the centre of the cylinder is therefore:

$$\boldsymbol{M}_{/O'} = 2\pi\mu UkR\sqrt{\frac{2R}{h}}\boldsymbol{k} = 2\pi\mu\Omega R^2\sqrt{\frac{2R}{h}}\boldsymbol{k}. \tag{3.26}$$

The fact that drag D is only due to the translation and the torque only to the rotation is in agreement with the results of Wakiya (1975) and Jeffrey & Onishi (1981), but Wakiya erroneously gave a drag proportional to $(2R/h)^{3/2}$ in contradiction to ours and that obtained by Jeffrey for $k = 0$ and 1.

It is now possible to give a good approximation (at order $O(\sqrt{h/R})$) of the pressure and viscous contributions. Since the torque due to pressure is zero at the centre of the cylinder, this torque at point O is $M_{p/O} = (D_p(R + h))$ where D_p is the pressure drag modulus. But we know from (2.28) that the viscous torque at point O tends towards the finite value $\mathscr{M}_{c/O}$ for h tending towards zero. We have therefore

$$\boldsymbol{M}_{/O} - \boldsymbol{M}_{p/O} - \boldsymbol{M}_{c/O} = O(h/R) \tag{3.27}$$

from which we can deduce the contributions of pressure and viscosity:

$$\boldsymbol{D}_p = -\left(2\pi\mu U(k+1)\sqrt{\frac{2R}{h}} + 4\pi\mu U(2k+1) + O(\sqrt{h/R})\right)\boldsymbol{i} \tag{3.28}$$

$$\boldsymbol{D}_v = \left(2\pi\mu Uk\sqrt{\frac{2R}{h}} - 4\pi\mu U(2k+1) + O(\sqrt{h/R})\right)\boldsymbol{i} \tag{3.29}$$

$$\boldsymbol{M}_{p/O} = \left(2\pi\mu U(k+1)(R+h)\sqrt{\frac{2R}{h}} - 4\pi\mu U(2k+1)R + O(\sqrt{h/R})\right)\boldsymbol{k} \tag{3.30}$$

$$\boldsymbol{M}_{V/O} = \left(4\pi\mu U(2k+1)R + O(\sqrt{h/R})\right)\boldsymbol{k}. \tag{3.31}$$

The numerical computation corroborates these analytical results as shown in figure 9.

3.4. *Forces and torque for non-zero Reynolds numbers*

At higher Reynolds numbers, the effect of the wake becomes sensitive, first to the lift that is zero only if $Re = 0$ but also to the drag. Taking the classical definition of the drag coefficient: $C_D = F_D/\rho U^2 R$, (3.22) becomes

$$C_D = \frac{4\pi}{Re}\sqrt{\frac{2R}{h}}. \tag{3.32}$$

Formula (3.32) can be compared with the numerical simulations of Stewart *et al.* (2010) and explains, at least for the lowest Reynolds numbers, why these authors noticed a weak influence of k compared with the effect of h. Present results show clearly that, for any Reynolds number, the rotation has no effect on the drag owing to the interstice that is dominant for low Reynolds numbers. For example for $Re = 20$ (the lowest Reynolds number discussed by Stewart *et al.*), formula (3.32) gives $C_D = 9.93$ for $h/2R = 4 \times 10^{-3}$, which is near the value found numerically by these authors: $C_D \approx 11$ to 12. According to our own results for $h/R = 0.005$ and $Re = 20$, the contribution of the wake is less than 10 % of the total drag. Stewart *et al.*estimated that the decrease of C_D versus h could be fitted to a power law of exponent -0.41 instead of 0.5 for the pure interstitial drag (3.32). Hence for $Re = 200$ (3.32) gives $C_D \approx 1$ equivalent to about one-half to one-third of the value found in

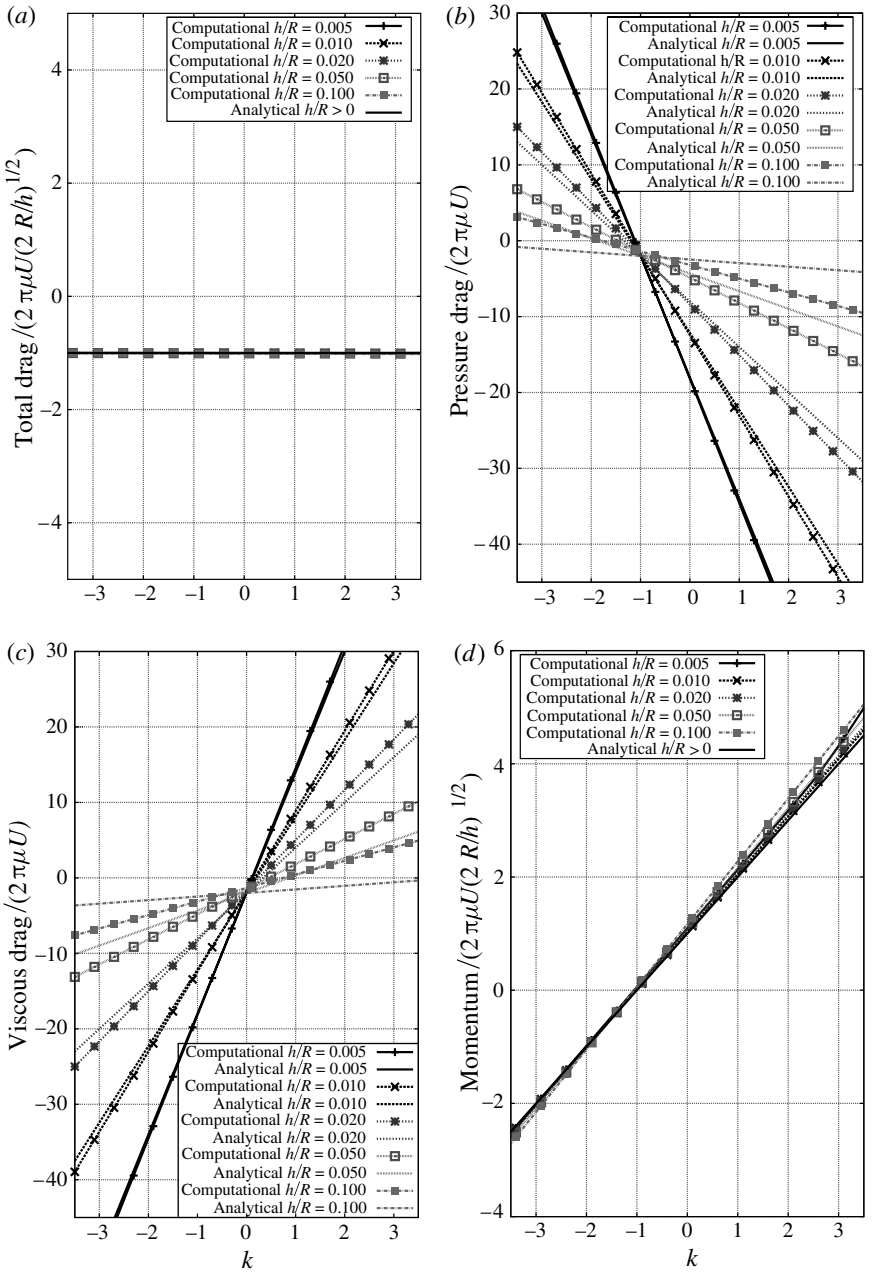

FIGURE 9. Numerical and analytical drag and torque versus k for different ratios h/R: (a) total drag, (b) pressure drag, (c) viscous drag, (d) total momentum. The total drag is remarkably constant and the agreement between numerical simulation and analytical prediction is perfect. The pressure and viscous drag are well predicted by the analytical approximations (3.28) and (3.29). It can be seen that when h increases the simulation and the analytical prediction tend to diverge as expected since the analytical formula are precise at order $O(h)$. Similar reasoning leads to an identical conclusion for the total momentum.

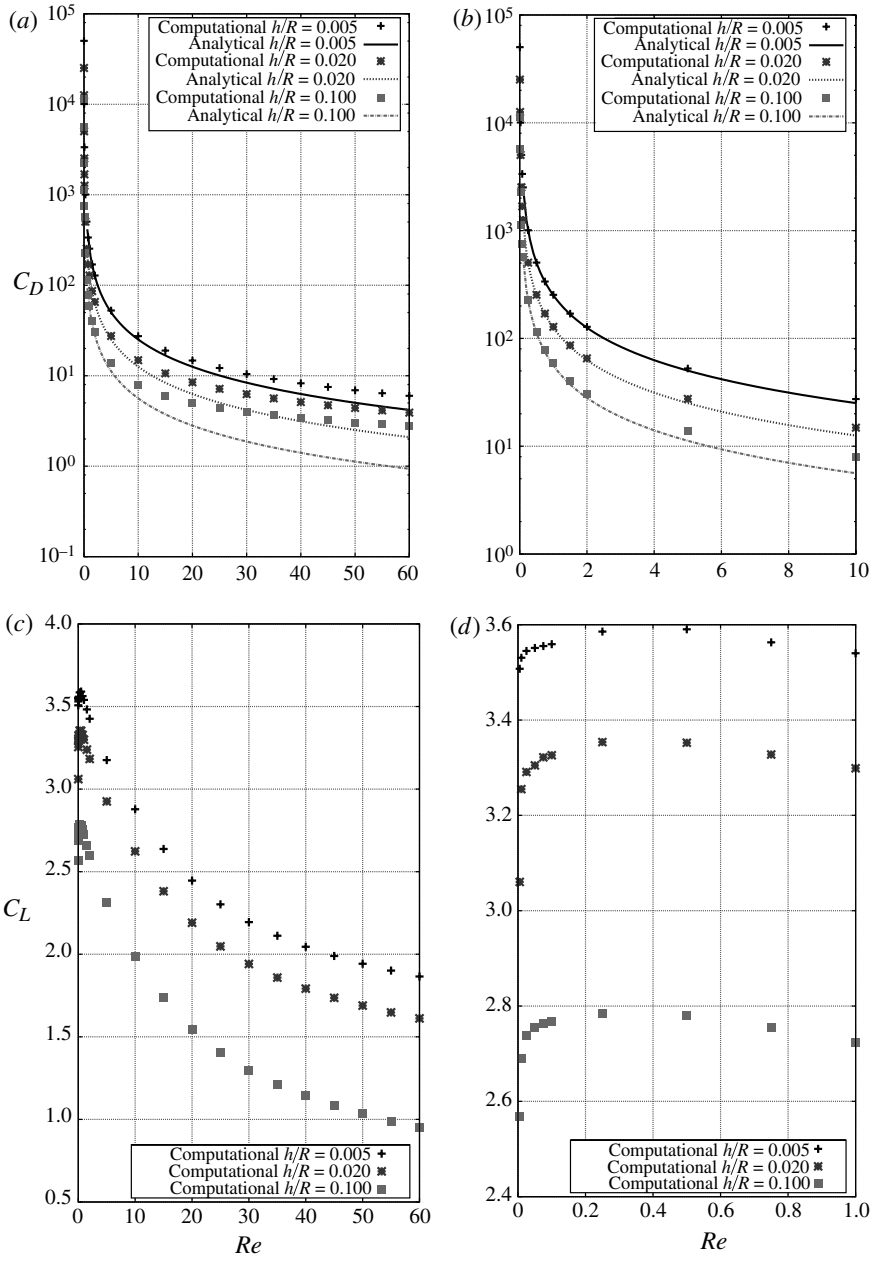

FIGURE 10. Numerical and theoretical values of the drag (*a*,*b*) and lift (*c*,*d*) coefficients for different values of h/R for $k = 1$. Analytical curves in (*a*) and (*b*) give the effect of the interstice alone (formula (3.32)), and (*b*) shows a good agreement between theory and numerical results at very low Reynolds numbers when the wake is not fully developed. At higher Reynolds number, the difference increases because theoretical curves correspond to the effect of the interstice alone. The lower h/R is, the higher is the drag induced by the interstice. The lift is entirely due to the asymmetry of the wall pressure on the cylinder induced by the wake. The lift coefficient increases continuously as Re decreases (*c*) but for $Re \ll 1$ (*d*) the lift coefficient drops suddenly towards zero as expected since in the Stokes flow regime, the lift is zero, at least in the absence of cavitation or compressible effects.

Stewart *et al.* (2010), suggesting a relative decrease of the interstitial contribution to the global drag.

As a significant example, figures 10 depict the variation of drag and lift coefficients versus Reynolds number between $Re = 0$ and $Re = 60$ for $k = 1$ and different values of h/R. Figure 10(*b*) shows the validity of formula (3.32) at low Reynolds number. As already mentioned in a previous section, the interstitial flow is independent of the external Reynolds number as long as the lubrication equation is valid; therefore (3.22) and (3.32) still fit for high values of Re but only represent the contribution of the interstice to the total drag. This contribution is prominent as long as the wake is not fully developed. A wider range of Re is displayed on figure 10(*a*), allowing the evaluation of the difference between the total drag obtained numerically and the interstitial contribution obtained analytically. This difference measures the wake contribution to the drag. These numerical results match perfectly with those of Stewart *et al.* (2010) and extend them to very low Reynolds numbers.

Figures 10(*c*) and 10(*d*), underline more specifically that the lift coefficient increases when Re decreases whereas it is supposed to be zero in the Stokes regime. Figure 10(*d*) depicts the lift behaviour for $0 < Re < 1$; it can be seen that the decline to zero is very sharp and that the Stokes regime around the rolling cylinder is very singular. This is because, even in presence of an interstitial flow, the lift is entirely due to the asymmetry of the flow, particularly because of the wake, which only vanishes in the Stokes regime.

3.5. *Description of the flow for a completely flooded interstice*

Once q^* has been determined all features of the flow can be defined. Let us first summarize the solution in the interstice:

$$\bar{\Psi} = \frac{\Psi}{Uh} = \frac{(k+1)}{3}\left(1 - \frac{3x^2}{2Rh}\right)\frac{y^3}{y_c^3} - \left(k - \frac{(k+2)x^2}{2Rh}\right)\frac{y^2}{y_c^2} - \frac{y}{h} \tag{3.33a}$$

$$\frac{u_x}{U} = (k+1)\left(1 - \frac{3x^2}{2Rh}\right)\frac{hy^2}{y_c^3} - 2\left(k - \frac{(k+2)x^2}{2Rh}\right)\frac{y}{y_c} - 1 \tag{3.33b}$$

$$\frac{v_y}{U} = \frac{xy^2}{Ry_c^2}\left(2(k+1)\frac{y}{y_c} - (3k+2)\right) \tag{3.33c}$$

$$p = \frac{2\mu U(k+1)}{h^2}\frac{x}{\left(1 + \dfrac{x^2}{2Rh}\right)^2} \tag{3.33d}$$

$$Q = -\frac{2}{3}(k+1)Uh. \tag{3.33e}$$

It is worthwhile underlining that the interstitial flow Q does not depend on the fluid properties. Even more remarkable is the position x_A of the pressure extrema where the pressure gradient is zero. $A = 0$, corresponds to $q_A = -(k+1)/2$ and therefore $x_A/h = \pm\sqrt{(2/3)(R/h)}$, which only depends on the geometry and not on any characteristic of the flow! Any change in the flow conditions (rotation (k), translation (U) or Re) for a given geometry, only induces a modification of the pressure gradient between these two fixed points that is to say, in pressure extrema variation. The pressure gradient at $x = 0$ is $A_0 = (2(k+1)\mu U)/h^2$ and the extremum pressure

$$p_M = \frac{3\sqrt{3}|k+1|}{4\sqrt{2}}\frac{\mu U}{h}\sqrt{\frac{R}{h}} \tag{3.34}$$

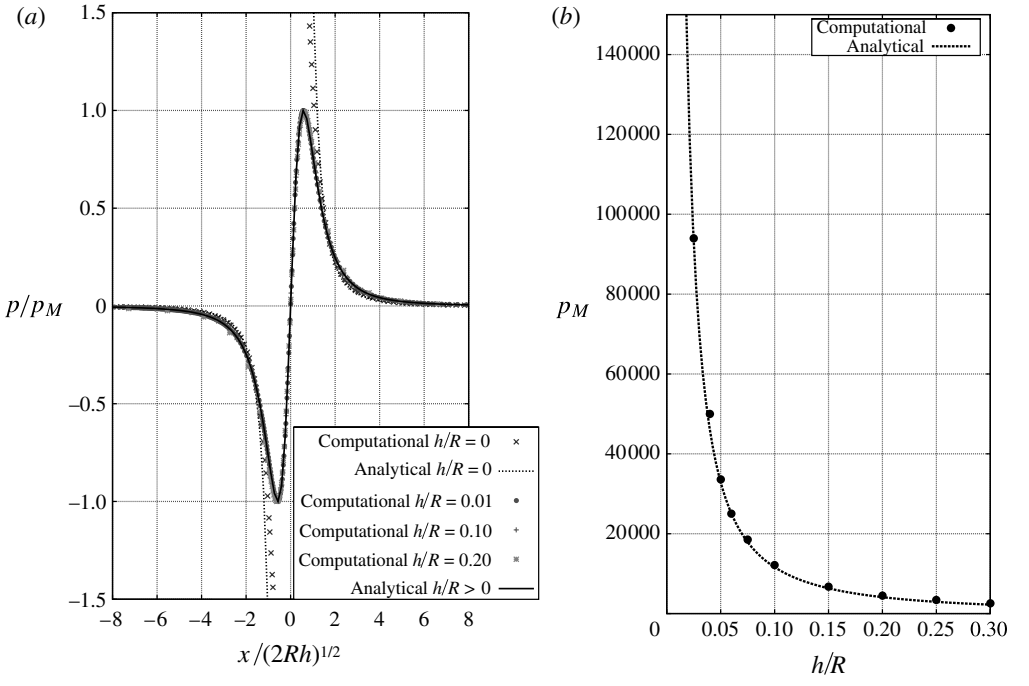

FIGURE 11. Pressure distribution in the interstice. Comparison between numerical and analytical results: (*a*) normalized pressure repartition p/p_M; (*b*) maximum pressure p_M. All computed cases for $h \neq 0$ fit with (3.35) and (3.34) while $h = 0$ compares the numerical pressure repartition with (2.18).

with the maximum downstream at $x_A = -\sqrt{(2/3)Rh}$ if $k > -1$ and upstream at $x_A = \sqrt{(2/3)Rh}$ if $k < -1$. Obviously, the minimum pressure $p_{min} = -p_M$ is located symmetrically. Except for $k = -1$ where $p = 0$ for all x, the pressure distribution in the interstice is given by the universal function

$$\frac{p}{p_M} = \frac{16}{3\sqrt{3}} \frac{X}{(1+X^2)^2} \tag{3.35}$$

where $X = x/\sqrt{2Rh}$ (figure 11).

For a good description of the interstitial flow it is necessary to localize the stagnation points. As a first step, let us identify curve C_u where $u_x = 0$. From (3.7),

$$Y = \frac{(3q + k + 2) \pm \sqrt{9q^2 + 6q(k+1) + k^2 + k + 1}}{3(2q + k + 1)} \tag{3.36}$$

which is a real two-branch function if $9q^2 + 6q(k+1) + k^2 + k + 1 > 0$. In the far field where $q \to 0$, the lower branch C_u^- is always in the flow $0 < Y < 1$ whereas it is the case for the upper branch only if $k > 0$. Figure 12 presents an example of C_u for $k = 1$ and $h/R = 0.025$.

For $k > 0$ the junction point of both branches corresponds to $q = q_u = -(k+1)/3 + \sqrt{k}/3$. Therefore, since $q^* < q_u < 0$, for $k > 0$ and $x > 0$ the two branches come from $x = \infty$ and join each other at $x = x_u = \sqrt{2((q^*)/(q_u) - 1)Rh} > 0$. A symmetrical curve exists for $x < 0$. For a stagnation point to exist on C_u, equation $v_y = 0$ must hold for

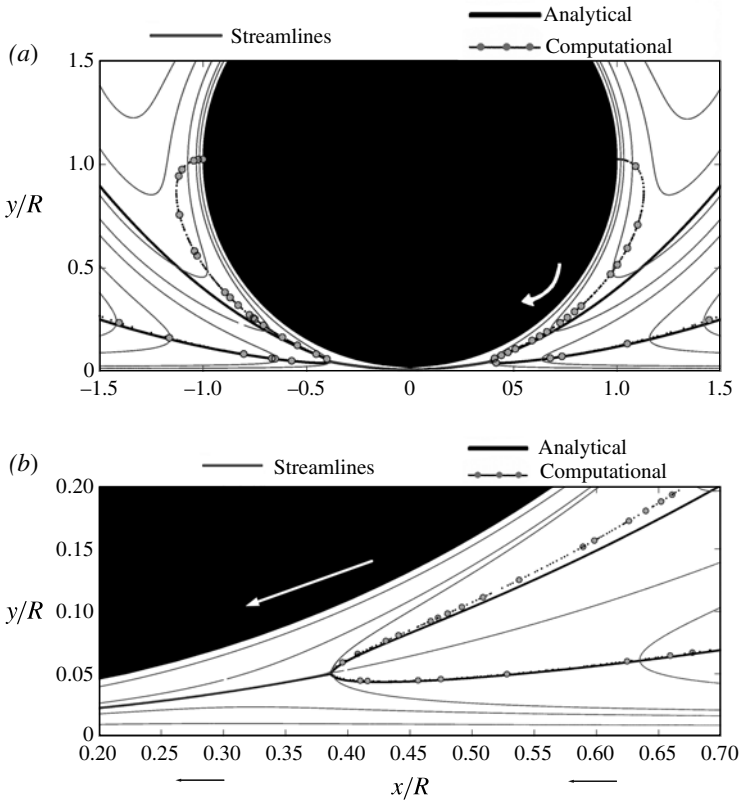

FIGURE 12. Upstream curve C_u (analytical (3.36) and numerical) and streamlines for $k = 1$ and $h/R = 0.025$: (*a*) global view; (*b*) close-up of the interstice. Both analytical C_u and numerical curves coincide, in the vicinity of the two-branch junction and near the wall. This coincidence increases if the dimensionless interstice size h/R decreases. Curve C_u is the location where streamlines turn back upstream, with a behaviour similar to a jet around line $Y = 1/2$ that corresponds, in the Stokes regime, to the external boundary of the vortex structure. Downstream from the nip, the feature is the same as in the Stokes regime but the fluxes are inverted. At higher global Reynolds numbers ($Re \gg 1$), the interstice feature is identical but the fit with the external flow is modified, particularly downstream.

$x \neq 0$ and $0 < Y < 1$. Taking (3.8) into account, this leads to

$$Y = \frac{6q + k + 2}{2(3q + k + 1)}. \tag{3.37}$$

The physical solution q_{st} of the system (3.36) and (3.37) is the root of the polynomial equation

$$\begin{aligned} &\left(18q^2 + 12q(k+1) + (k+1)(k+2)\right)^2 \\ &\quad = 4(3q + k + 1)^2(9q^2 + 6q(k+1) + k^2 + k + 1) \end{aligned} \tag{3.38}$$

that fulfils the requirements $0 < Y < 1$ and $q_u < q < 0$. This solution is

$$q_{st} = -\frac{k+1}{3} + \frac{1}{6}\sqrt{8 + 2k + 2k^2 - 4\sqrt{(k-1)^2 + k^2 + 3}}. \tag{3.39}$$

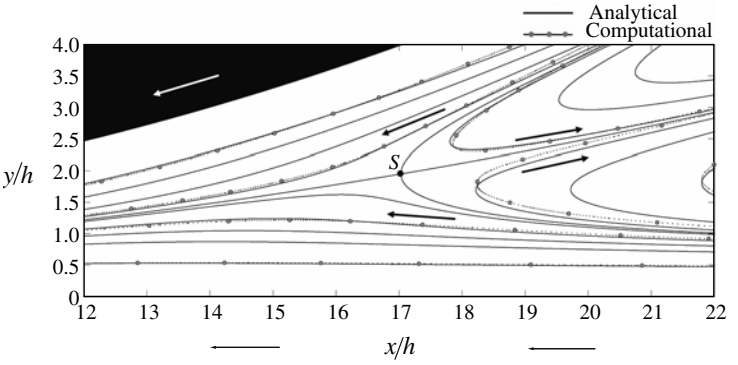

FIGURE 13. Streamlines of the interstitial flow for $k = 1$. Close-up of the upstream stagnation point area. The flow is the confluence of two equal fluxes, one dragged by the cylinder and the other by the wall. Around the upstream stagnation point, the part of the flow that cannot enter the interstice is ejected upstream on both sides of a central line that corresponds to the external boundary of the vortex structure. Of these streamlines, those located above this central line are trapped in the vortex structure, the others turn around the vortex and reach the downstream stagnation point area before continuing at $x \to -\infty$.

In the case $k = 1$, since $q_u = q_{st} = -1/3$ and $Y_{st} = 1/2$, the stagnation point is located just at the junction of the two branches of C_u (figure 13) at $x_{st} = \sqrt{2Rh}$ (figure 14). This location corresponds exactly to points $x_{A'}$ where the pressure gradient derivative is zero.

For $k > 1$ the stagnation points S are located on the lower branch of C_u and for $k < 1$ on the upper one (figures 15*a* and 15*b*). These stagnation points behave as saddle points where the flow driven by the cylinder meets the flow driven by the wall before entering the interstice or being pushed back around the cylinder.

For $k = 0$, it is easy to verify that the upper branch of C_u (3.36) degenerates to $Y = 1$ for all q since the velocity is zero on the cylinder. In that case, we have $q_u = q_{st} = -1/3$, and $Y_u = Y_{st} = 1$. This means that the lower branch of C_u ends on the cylinder surface at $x_{st} = x'_A = \sqrt{2Rh}$ (figure 16). This location of the stagnation points for $k = 0$ was already obtained theoretically in Jeffrey & Onishi (1981) and numerically in Stewart *et al.* (2010).

For $k < 0$ and $k \neq -1$, curve C_u is reduced to its lower branch that exists for any value of q and is therefore continuous in the interval $-\infty < x < \infty$. Moreover, no root of (3.38) fulfils condition $0 \leqslant Y < 1$. Therefore, v_y is zero only for $x = 0$. As a consequence, $q_{st} = q^*$ and, according to (3.36), the stagnation point is located at

$$Y_{st} = \frac{k + \sqrt{k^2 + k + 1}}{k + 1}, \quad x_{st} = 0. \tag{3.40}$$

The general features for $k < 0$ are given figure 17. The case $k = -1$ is singular because (3.7) degenerates into $q = q^* = 0$. The solution becomes $q = 0$ for all x and curve C_u reduces simply to $Y = 1/2\ \forall x$.

It is now possible to determine the rate difference between the flow driven by the wall and that driven by the cylinder in the interstice. The flow rate driven by the wall is simply given by the value of the stream function Ψ_{st} at the stagnation point. Moreover, $\Psi = \Psi_{st}$ corresponds to the streamline that separates the flow driven by the wall and passing through the interstice from the flow turning around the cylinder.

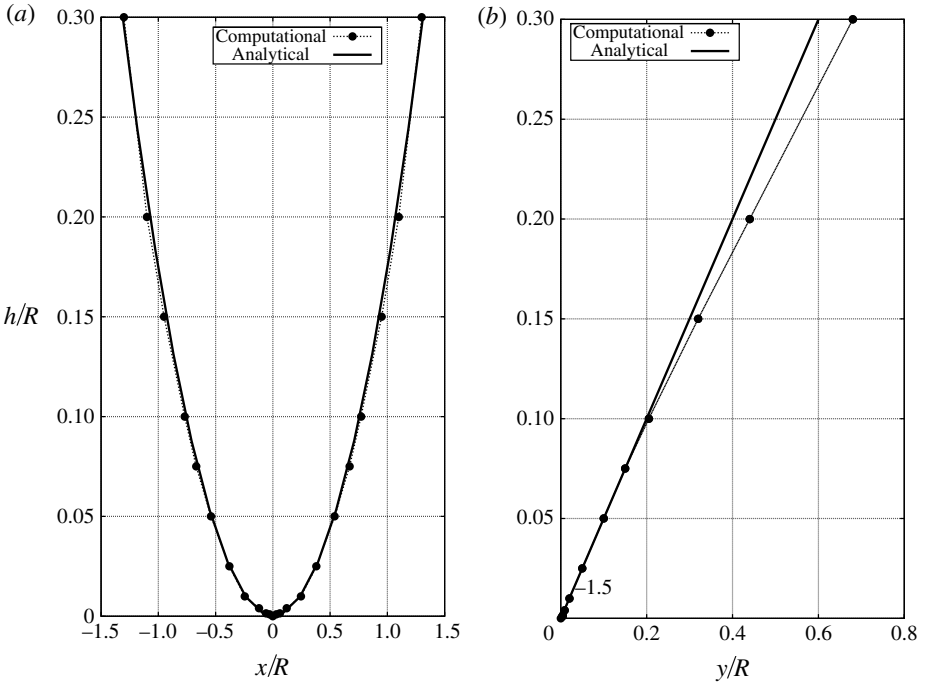

FIGURE 14. Position of stagnation points for $k = 1$. Comparison between analytical and numerical results, for varying h/R: (a) x/R and (b) y/R. Analytical and numerical predictions coincide until $h/R > 0.1$.

According to (3.33a), the value of Ψ_{st} for $x \to \infty$, $q \to 0$ and $y/y_c \to 0$ is equal to the ratio $-y_\infty/h$ where y_∞ is the thickness of the fluid film driven by the wall and passing through the interstice:

$$\frac{y_\infty}{h} = -\Psi_{st} = -\Psi(x_{st}, q_{st}, Y_{st}) \tag{3.41}$$

where, for $k \geqslant 0$, Y_{st} and q_{st} are given respectively by (3.37) and (3.39) and x_{st} by

$$x_{st} = \sqrt{2Rh\left(\frac{q^*}{q_{st}} - 1\right)}. \tag{3.42}$$

For $k < 0$, $x_{st} = 0$, $q_{st} = q^*$ and Y_{st} is given by (3.40). Tables 1 and 2 summarize these results for a few significant values of k.

For $k \geqslant 0$, table 1 provides the ratio Ψ_{st}/q^* between the flow driven by the wall and the global interstitial flow, while table 2, which covers $k < 0$ values, gives the ratio between the fluid driven downstream by the wall and the opposite flow driven upstream by the cylinder: $|\Psi_{st}|/|q^* - \Psi_{st}|$.

3.6. *Cavitation*

The familiar Reynolds conditions for cavitation are

$$A = \frac{\mathrm{d}p}{\mathrm{d}x} = 0 \quad \text{and} \quad p = 0. \tag{3.43}$$

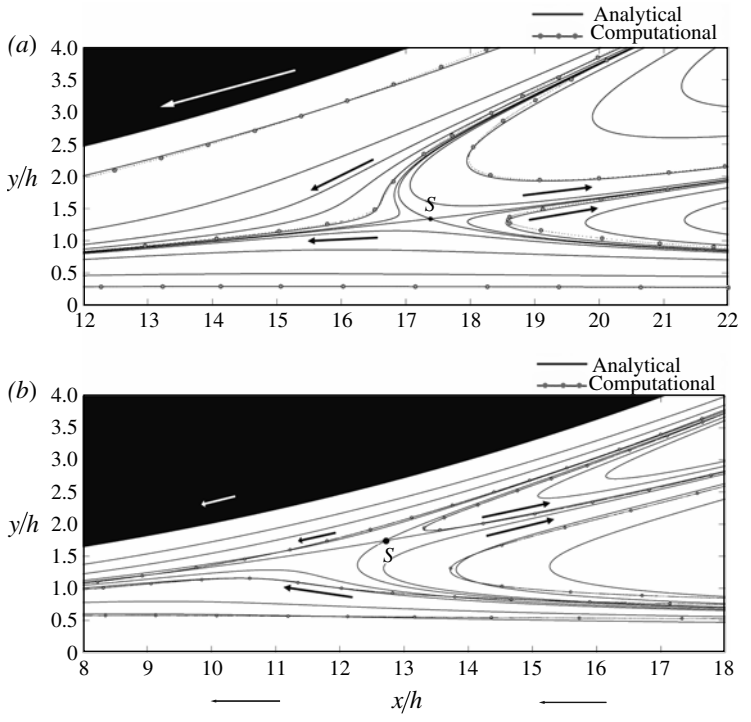

FIGURE 15. Close-up of the vicinity of the upstream stagnation point S. Streamlines for (a) $k = 2$. The stagnation point is on the lower C_u branch. The downstream stagnation point can be deduced inverting the direction of the arrows. (b) $k = 0.5$. The stagnation point is on the upper branch of C_u.

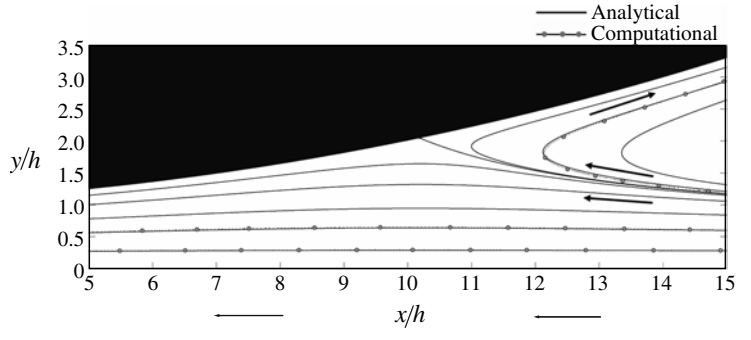

FIGURE 16. The particular case $k = 0$. Close-up of the stagnation point area. All the flow crossing the nip is driven by the wall, the upper branch or C_u is the cylinder itself where the velocity is zero. The flow that does not enter the nip turns around the cylinder and the vortex structure does not exist. The pattern is the same downstream but with inverted arrows.

Surface tension γ can be neglected if $\gamma/\mu U\sqrt{h/R} \ll 1$ (Savage 1982) which is always the case for h sufficiently small. The cavitation condition can be summarized as

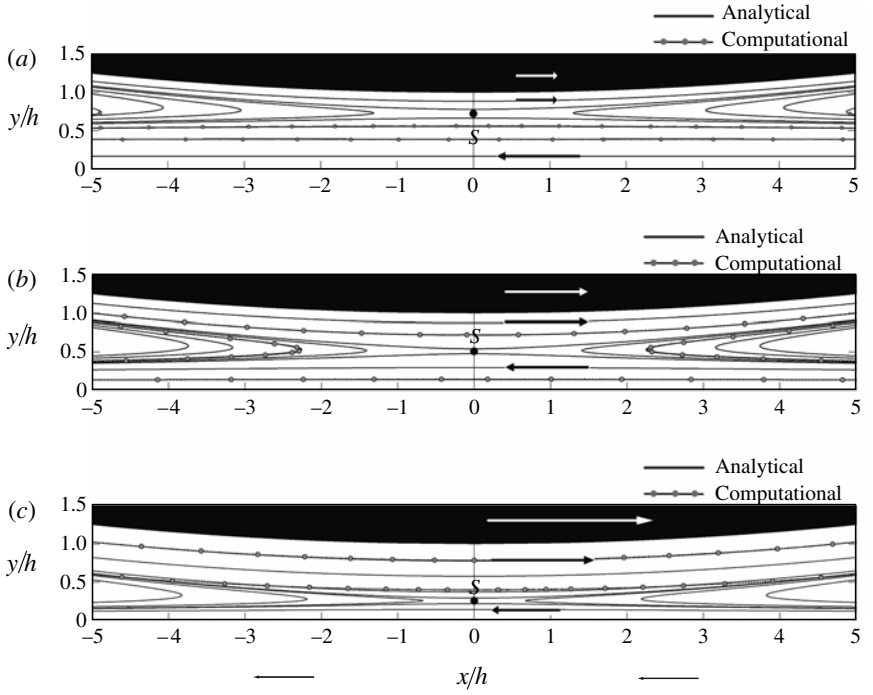

FIGURE 17. Interstitial flow for $k < 0$, two opposite flows are competing. (*a*) $k = -0.5$: the stagnation point position S ($Y_{st} = 0.732$) is given by (3.40). (*b*) $k = -1$: the two opposite flows are equal and therefore $q^* = 0$, $Y_{st} = 1/2$. (*c*) $k = -2$: (3.40) gives $Y_{st} = 0.268$, the flux driven upstream by the cylinder is higher than the flux driven downstream by the wall.

k	0	0.25	0.5	1	2	3	4
$x_{st}/\sqrt{2Rh}$	±1	±1.531	±1.673	±1.732	±1.712	±1.732	±1.774
Y_{st}	1	0.751	0.6479	1/2	0.321	0.250	0.228
y_∞/h	2/3	0.742	0.74	2/3	0.518	0.417	0.339
Ψ_{st}/q^*	1	0.891	0.74	1/2	0.259	0.156	0.102

TABLE 1. Prograde rotation. Line 1: x coordinates of stagnation points; line 2: y coordinates of stagnation points; line 3: thickness of the fluid film that enters the interstice, far upstream at the wall; line 4: ratio between the flow rate driven by the wall and the total flow rate in the interstice.

k	-3	-2	-1	-0.5
Y_{st}	0.177	0.268	1/2	0.732
y_∞/h	0.087	0.131	1/4	0.339
$\lvert\Psi_{st}\rvert/\lvert q^* - \Psi_{st}\rvert$	0.061	0.164	1	6.100

TABLE 2. Retrograde rotation. Line 1: y coordinates of stagnation points; line 2: thickness of the fluid film that enters the interstice, far upstream at the wall; line 3: ratio between the flow rates driven by the wall and the cylinder in the interstice.

k	-3	-2	-1	-0.5	0	1	2	3	4
q_0^* $(p_\infty = 0)$	1.225	0.6128	0	-0.306	-0.6128	-1.225	-1.8386	-2.452	-3.06
q_M^* $(p_\infty = p_M)$	1.333	0.667	0	-0.333	-0.667	-1.333	-2	-2.667	-3.333

TABLE 3. Limit values of $q^* = Q/Uh$ in the case of cavitation. For p_∞ growing from 0 to p_M cavitation happens with an increasing interstitial flow rate Q from $q_0^* Uh$ until the maximum value $q_M^* Uh$ for which cavitation disappears. For $p_\infty > p_M$ the interstice is totally flooded and the flow rate remains equal to $q_M^* Uh$.

follows:

$$\text{if } p_\infty < p_M = \frac{3\sqrt{3}|k+1|}{4\sqrt{2}} \frac{\mu U}{h} \sqrt{\frac{R}{h}} \text{ cavitation appears} \tag{3.44}$$

$$\text{if } p_\infty > p_M = \frac{3\sqrt{3}|k+1|}{4\sqrt{2}} \frac{\mu U}{h} \sqrt{\frac{R}{h}} \text{ the nip is totally flooded.} \tag{3.45}$$

Let us denote as x_{cav} the location of the minimum pressure ($A = 0$). At that abscissa we have $q = -(k+1)/2$ or, in terms of variable Z, $Z = Z_{cav} = (1 + x_{cav}^2/2Rh)^{-1} = -(k+1)/2q^*$. Because of the symmetry of $A(x)$, it is easier to replace equation $p(x_{cav}) = 0$ with the equivalent condition $p(0) = p(x_{max})/2$ or explicitly:

$$\begin{aligned} &\operatorname{sgn}(x_{max}) \frac{12\mu U}{h^2} \sqrt{\frac{Rh}{2}} \int_0^{-(k+1)/2q^*} \frac{\sqrt{Z}(q^* Z + (k+1)/2)}{\sqrt{1-Z}} \, \mathrm{d}Z + p_\infty \\ &\quad = 2\operatorname{sgn}(x_{max}) \frac{12\mu U}{h^2} \sqrt{\frac{Rh}{2}} \int_0^1 \frac{\sqrt{Z}(q^* Z + (k+1)/2)}{\sqrt{1-Z}} \, \mathrm{d}Z \end{aligned} \tag{3.46}$$

resulting after integration in:

$$\begin{aligned} &\left(\frac{3q^*}{4} + \frac{k+1}{2}\right) \left(\arcsin \sqrt{-\frac{k+1}{2q^*}} - \pi - \sqrt{-\frac{k+1}{2q^*}\left(1 + \frac{k+1}{2q^*}\right)} \right) \\ &\quad + \frac{k+1}{4} \sqrt{-\frac{k+1}{2q^*}\left(1 + \frac{k+1}{2q^*}\right)} - \operatorname{sgn}(q^*) \frac{p_\infty h^2}{12\mu U} \sqrt{\frac{2}{Rh}} = 0 \end{aligned} \tag{3.47}$$

since $\operatorname{sgn}(x_{max}) = -\operatorname{sgn}(q^*)$.

It is easy to verify that $q^* = -2(k+1)/3$ gives as expected $p_\infty = p_M$ (3.34). Solutions q^* of (3.47) appear to be monotonic growing functions of p_∞ for all k, in the range $[p_\infty = 0, p_\infty = p_M]$ where cavitation happens. Table 3 gives the limits of the cavitation domain $[q_0^*, q_M^*]$ versus k (q_0^* corresponding to $p_\infty = 0$ and $q_M^* = -2/3(k+1)$ to $p_\infty = p_M$). It is remarkable that the result is antisymmetrical relative to $k = -1$, which comes from the expression of p_M (3.34). The values of q_M^* and q_0^* for $k = 1$ were obtained by Taylor (1963) in a different way. Notice that case $k = -1$ is very particular since the flow rate is zero and moreover the relative pressure in the interstice is zero all along the wall.

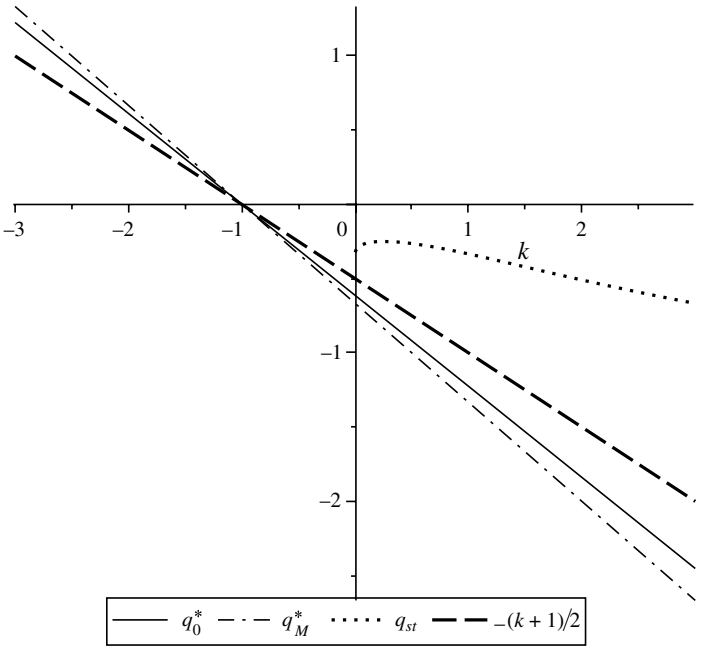

FIGURE 18. Comparison between q_{st} and $q_A = -(k+1)/2$ for $k > 0$ and between q_A and q_0^*, q_M^*. It is clear that $q_{st} > q_A$ for all $k > 0$ and that q_A is never in the domain limited by q_0^* and q_M^* corresponding to the possible value of q^* at the stagnation point $x = 0$ for $k > 0$.

The location of the cavitation point can be deduced from $q = -(k+1)/2 = q^*/(1 + x_A^2/2Rh)^2$:

$$x_{cav} = \mathrm{sgn}(q^*)\sqrt{-2\left(\frac{2q^*}{k+1} - 1\right)Rh}. \tag{3.48}$$

For a completely flooded interstice ($q^* = -2(k+1)/3$) this expression corresponds to x_A as expected.

It is remarkable that the cavitation inception x_{cav} does not takes place at the stagnation points. For $k \geqslant 0$ according to (3.42) and (3.48), the equality $x_{cav} = x_{st}$ would lead to $q_{st} = -(k+1)/2$ which is impossible since $q_{st}(k) > -(k+1/2)$ for all $k \geqslant 0$ (figure 18), and as a consequence: $-x_{st} < x_{cav} < 0$. For $k < 0$, condition $x_{st} = 0$ would lead to $q^* = -(k+1/2)$ but, as $-(k+1/2)$ never belongs to the domain limited by q_0^* and q_M^* except for $k = -1$ (figure 18), cavitation cannot appear at $x = 0$. These results show that, under the present assumptions ($\gamma/\mu U\sqrt{h/R} \ll 1$), a steady two-dimensional meniscus cannot occur in the interstice. The flow must become three-dimensional as confirmed in the experimental work by Taylor (1963) with Newtonian fluids and more recently by Ouibrahim, Fruman & Gaudemer (1996) for Newtonian and non-Newtonian fluids with no major differences. Moreover, if the cylinder is free to move under the effect of the lift force, an unsteady behaviour may occur as the periodic emission of bubbles that appear in experiments (Seddon & Mullin 2006).

As was seen previously, for $k < -1$ the cavitation appears upstream of the nip, and downstream for $k > -1$, but the case $k = -1$ is particular since the relative pressure in the interstice is $p = p_\infty$ in terms of absolute pressure, there are no pressure extrema and therefore no localized cavitation onset.

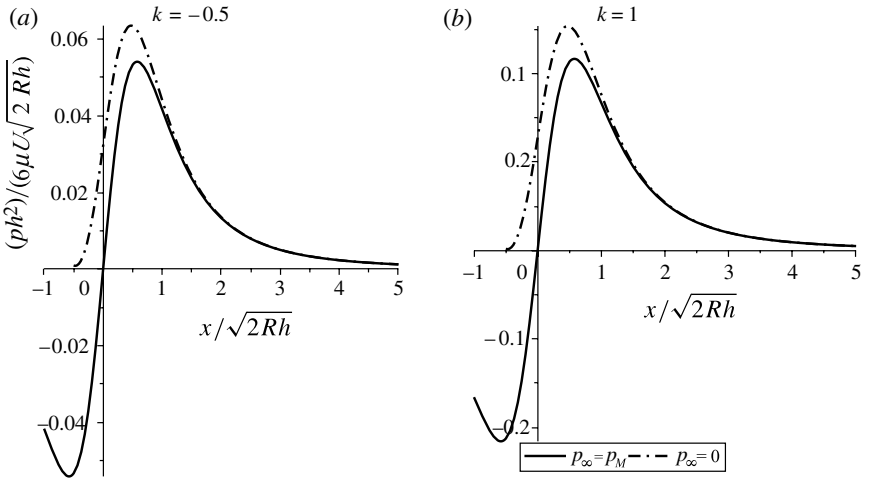

FIGURE 19. Pressure repartitions in the interstice for $p_\infty = 0$ and $p_\infty = p_M$ and negative values of q^*. Similar figures for $q^* > 0$ ($k < -1$) can be obtained by changing x to $-x$ while k is changed to $-(k+2)$. The maximum pressure increases with k as expected from (3.34). Cavitation slightly increases this maximum. The cavitation location is always very near to $x = -\sqrt{Rh}$. The exact values for the case $p_\infty = p_M$ is $x_{cav}/\sqrt{2Rh} = x_A/\sqrt{2Rh} = -\sqrt{1/3} \approx -0.577$ which does not depend on k. For $p_\infty = 0$, $x_{cav}/\sqrt{2Rh}$ is 0.473 for $k = -0.5$ (a), 0.474 for $k = 1$ (b).

In all cases, the relative pressure can be obtained by

$$p(x) = \mathrm{sgn}(x)\frac{12\mu U}{h^2}\sqrt{\frac{Rh}{2}}\int_0^{(1+(x^2/2Rh))^{-1}} \frac{\sqrt{Z}\,(q^*Z + (k+1)/2)}{\sqrt{1-Z}}\,\mathrm{d}Z + p(0) \quad (3.49)$$

where

$$p(0) = -\mathrm{sgn}(q^*)\frac{3\pi\mu U}{h^2}\sqrt{2Rh}\left(\frac{3}{4}q^* + \frac{k+1}{2}\right) + p_\infty. \quad (3.50)$$

Figure 19 depicts examples of the relative pressure repartition $p - p_\infty$ in the interstice for $q^* < 0$ (i.e. $-1 < k$). Similar figures for $q^* > 0$ ($k < -1$) can be obtained by changing x to $-x$ while k is changed to $-(k+2)$. The case $p_\infty = p_M$ corresponds to a flow without cavitation, the case $p_\infty = 0$ is the upper limit for cavitation flows. For intermediate values of p_∞ the pressure repartition is located between these two curves. It can be seen that the maximum relative pressure increases slightly when cavitation appears. It is also shown that x_{cav} is always very close to $-\sqrt{Rh}$ since, for all $k > -1$, it varies from $-0.577\sqrt{2Rh}$ for $p_\infty = p_M$ to approximately $0.474\sqrt{2Rh}$ when p_∞ decreases to zero.

4. Conclusion

The two-dimensional Stokes flow around a cylinder rolling on a plate was solved for any translation and rotation velocity of the cylinder and with a perfect contact. Agreement between the Stokes solutions and the full Navier–Stokes numerical simulations at $Re \ll 1$ is excellent and computations at higher Reynolds numbers are in total agreement with those of Stewart *et al.* (2010). A vortex structure is shown to appear for prograde rotation in the Stokes regime. This vortex is converted

progressively into a wake when the Reynolds number increases, and at about $Re = 40$ a second vortex is therefore generated in the wake, in the vicinity of the wall.

A pathologic problem of the Stokes solutions was detected at the contact point where the upstream pressure tends toward $+\infty$ and the downstream pressure tends towards $-\infty$. Therefore, for realistic stagnation pressures, there is no solution of the incompressible Navier–Stokes equations. Compressibility or cavitation must occur systematically near the contact point, limiting the pressure drop to a physically acceptable value. This results in an infinite lift force that opens an interstice between the wall and the cylinder. The flow in the completely flooded interstice was solved analytically within the theory of lubrication and stream functions were obtained for all configurations. A detailed description of the flow field inside the interstice was therefore provided, giving the location of stagnation points and the thickness of the far-field layer coming along the wall and entering the interstice. The drag and the torque applied on the cylinder were determined analytically and compared with computations for different heights of the interstice and Reynolds numbers, clarifying some discrepancies in the literature.

A global model of the interstice was deduced allowing its treatment as a contact point but with a non-zero flow and where point forces and a torque are applied on the wall and the cylinder. This global concept of the interstice can be very useful for modelling small gaps between two-dimensional boundaries.

Drag and torque were studied in detail for the Stokes flow around the cylinder in order to separate the effect of pressure and viscosity, but also the respective influence of the body and the interstice. At higher Reynolds numbers, the lift force was also studied numerically for $0 < Re < 40$. It is shown that the lift coefficient increases when Re decreases except for $Re \ll 1$ where it undergoes a sudden decay to zero as expected for the Stokes regime.

Finally, the study of the conditions for cavitation inception in the interstice enabled the determining of the location of the onset of cavitation and the correlative fluxes. It is shown that these locations are never identical to those of stagnation points and that, consequently, when cavitation appears, the flow must become three-dimensional downstream from the cavitation onset.

Further research can take advantage of the present punctual model of interstices, not only for finding analytical Stokes flows in configurations including cylinders, but also for simplifying the mesh strategy in two-dimensional computations with small gaps between solid boundaries. This can be helpful for treating problems related to micropumps based on cylinder rotations, squeezed thin films or aquaplaning since the interstitial flow is not limited to small Reynolds numbers.

REFERENCES

ABDELGAWAD, M., HASSAN, I. & ESMAIL, N. 2003 Transient behaviour of the viscous micropump. *Microscale Therm. Engng* **8**, 361–381.

ABDELGAWAD, M., HASSAN, I., ESMAIL, N. & PHUTTHAVONG, P. 2005 Numerical investigation of multistage viscous micropump configurations. *Trans. ASME: J. Fluids Engng* **127**, 734–742.

ASHMORE, J., DEL PINO, C. & MULLIN, T. 2005 Cavitation in a lubrication flow between a moving sphere and a boundary. *Phys. Rev. Lett.* **94**, 124501.

BALLAL, B. Y. & RIVLIN, R. S. 1976 Flow of a Newtonian fluid between eccentric rotating cylinders: inertial effects. *Arch. Rat. Mech. Anal.* **62** (3), 237–294.

BEARMAN, P. W. & ZDRAVKOVICH, M. M. 1978 Flow around a circular cylinder near a plane boundary. *J. Fluid Mech.* **89**, 33–47.

BHATTACHARYYA, S., MAHAPATRA, S. & SMITH, F. T. 2004 Fluid flow due to a cylinder rolling along ground. *J. Fluids Struct.* **19**, 511–523.

CHAUVEAU, F. 2002 Aérodynamique de l'avant corps d'une formule 1: Approche numérique. Thèse de doctorat (in French), Univ Sc. Tech. Lille1. France.

CHENG, M. & LUO, L. S. 2007 Characteristics of two-dimensional flow around a rotating circular cylinder near a plane wall. *Phys. Fluids* **19**, 063601.

CHOI, H. I., LEE, Y. & CHOI, D. H. 2010 Design optimization of a viscous micropump with two rotating cylinders for maximizing efficiency. *Struct. Multidisc. Optim.* **40**, 537–548.

COYLE, D. J., MACOSKO, C. W. & SCRIVEN, L. E. 1986 Film-splitting flows in forward roll coating. *J. Fluid Mech.* **171**, 183–207.

DAY, R. F. & STONE, H. A. 2000 Lubrification analysis and boundary integral simulations of a viscous micropump. *J. Fluid Mech.* **416**, 197–216.

DECOURTYE, D., SEN, M. & GAD-EL-HAK, M. 1998 Analysis of viscous micropumps and microturbines. *Intl J. CFD* **10**, 13–25.

DIPANKAR, A. & SENGUPTA, T. K. 2005 Flow past a circular cylinder in the vicinity of a plane wall. *J. Fluids Struct.* **20** (3), 403–423.

FINN, M. D. & COX, S. M. 2001 Stokes flow in a mixer with changing geometry. *J. Engng Maths* **41**, 75–99.

GASKELL, P. H., SAVAGE, M. D., SUMMERS, J. L. & THOMPSON, H. M. 1995 Modelling and analysis of meniscus roll coating. *J. Fluid Mech.* **298**, 113–137.

GASKELL, P. H., SAVAGE, M. D. & THOMPSON, H. M. 1998 Stagnation-saddle points and flow patterns in Stokes flow between contra-rotating cylinders. *J. Fluid Mech.* **370**, 221–247.

HUANG, W. X. & SUNG, H. J. 2007 Vortex shedding from a circular cylinder near a moving wall. *J. Fluids Struct.* **23**, 1064–1076.

JEFFREY, D. J. & ONISHI, Y. 1981 The slow motion of a cylinder next to a plane wall. *Q. J. Mech. Appl. Maths* **34**, 129–137.

JEFFERY, G. B. 1922 The rotation of two circular cylinders in a viscous fluid. *Proc. R. Soc. Lond.* A **101**, 169–174.

KANO, I. & YAGITA, M. 2002 Flow around a rotating circular cylinder near a moving plane wall. *JSME Intl J.* B **45** (2), 259–268.

MATTHEWS, M. T. & HILL, J. M. 2006 Lubrication analysis of the viscous micro/nano pump with slip. *Microfluid. Nanofluid.* **4**, 439–449.

MATTHEWS, M. T. & HILL, J. M. 2009 Asymptotic analysis of the viscous micro/nano pump at low Reynolds number. *J. Engng Maths* **63** (2), 279–292.

MOFFATT, H. K. 1964 Viscous and resistive eddies near a sharp corner. *J. Fluid Mech.* **18**, 1–18.

NISHINO, T., ROBERTS, G. T. & ZHANG, X. 2007 Vortex shedding from a circular cylinder near a moving ground. *Phys. Fluids* **19**, 025103.

OUIBRAHIM, A., FRUMAN, D. H. & GAUDEMER, R. 1996 Vapour cavitation in very confined spaces for Newtonian and non Newtonian fluids. *Phys. Fluids* **8** (7), 1964–1971.

SAVAGE, M. D. 1982 Mathematical models for coating processes. *J. Fluid Mech.* **117**, 443–445.

SCHUBERT, G. 1967 Viscous flow near a cusped corner. *J. Fluid Mech.* **27**, 647–656.

SEDDON, J. R. T. & MULLIN, T. 2006 Reverse rotation of a cylinder near a wall. *Phys. Fluids* **18**, 041703.

SEN, M., WAJERSKI, D. & GAD-EL-HAK, M. 1996 A novel pump for MEMS application. *J. Fluids Engng* **118**, 624–627.

SHARATCHANDRA, M. C., SEN, M. & GAD-EL-HAK, M. 1997 Navier–Stokes simulation of a novel viscous pump. *J. Fluids Engng* **119**, 372–382.

SHARATCHANDRA, M. C., SEN, M. & GAD-EL-HAK, M. 1998 Thermal aspects of a novel viscous pump. *J. Heat Transfer* **120**, 99–107.

STEWART, B., HOURIGAN, K., THOMPSON, M. & LEWEKE, T. 2006 Flow dynamics and forces associated with a cylinder rolling along a wall. *Phys. Fluids* **18**, 111701.

STEWART, B., THOMPSON, M., LEWEKE, T. & HOURIGAN, K. 2010 The wake behind a cylinder rolling on a wall at varying rotation rates. *J. Fluid Mech.* **648**, 225–256.

TAYLOR, G. I. 1963 Cavitation of a viscous fluid in narrow passages. *J. Fluid Mech.* **16**, 595–619.

WAKIYA, S. 1975 Application of bipolar coordinates to the two-dimensional creeping motion of a liquid. Part II. *J. Phys. Soc. Japan.* **39** (6), 1603–1607.

ZDRAVKOVICH, M. M. 1982 Forces on a circular cylinder near a plane wall. *J. Appl. Ocean Res.* **7** (4), 197–201.